

Doping effects in AlGaAs lasers with separate  
confinement heterostructures (SCH).  
Modeling optical and electrical characteristics  
with Sentaurus TCAD.

Z. Koziol,\* and S. I. Matyukhin,

Orel State Technical University,

29 Naugorskoye Shosse, Orel, 302020, Russia.

**Abstract**

Optical and electrical characteristics of AlGaAs lasers with separate confinement heterostructures are modeled by using Synopsys's Sentaurus TCAD and open source software for semi-automatic data analysis of large collections of data. The effects of doping in all laser layers are investigated with the aim to achieve optimal characteristics of the device. The results are compared with those obtained for real lasers produced at Polyus research institute in Moscow, showing that a significant improvement can be achieved, in particular an increase in optical efficiency (up to over 70 %) by careful control of type and level of doping throughout the entire structure.

---

\*Corresponding author email: zbigniew@ostu.ru

# Contents

<b>1</b>	<b>Introduction</b>	<b>3</b>
<b>2</b>	<b>Lasers structure and calibration of modeling.</b>	<b>4</b>
<b>3</b>	<b>Methods of data analysis.</b>	<b>7</b>
3.1	Using Perl, TCL, gnuplot, and other open source tools on Linux.	7
3.2	Threshold current and $L(I)$ dependence. . . . .	7
3.3	Three ways of finding lasing offset voltage $U_0$ . . . . .	8
3.3.1	$U_0$ from fitting $U(I)$ dependence . . . . .	8
3.3.2	$U_0$ from maximum of $d\log L(U)/dU$ . . . . .	9
3.3.3	$U_0$ from gain versus voltage curves. . . . .	10
3.4	Differential resistance and optical efficiency. . . . .	10
<b>4</b>	<b>N-N waveguide structure.</b>	<b>12</b>
4.1	The role of doping in Active Region (QW). . . . .	12
4.2	The role of doping in Waveguide Regions. . . . .	17
4.3	The role of doping in Emitters Regions. . . . .	23
<b>5</b>	<b>N-P waveguide structure.</b>	<b>33</b>
5.1	Active region doping . . . . .	34
5.2	Waveguides doping . . . . .	36
5.3	Doping in Emitters . . . . .	40
<b>6</b>	<b>Summary and Conclusions.</b>	<b>46</b>

# 1 Introduction

An idea of Alferov et al., [1], comprising the use of a geometrically-narrow active recombination region where photon generation occurs (Quantum Wells; QW), with waveguides around improving the gain to loss ratio (separate confinement heterostructures; SCH), has largely dominated the field of optoelectronics development in the past years. AlGaAs edge emitting lasers are an example of practical realization of these ideas.

Now, they are mostly used for pumping solid state  $Nd : YAG$  lasers used either in high-power metallurgical processes or, already, in first field experiments as a highly directional source of energy in weapons interceptors.

In our earlier works we first were able to find agreement between our calculations of quantum well energy states and the lasing wavelength observed experimentally [2]. Next [3], several changes in structure of SCH AlGaAs lasers have been shown to considerably improve their electrical and optical parameters. We compared computed properties with these of lasers produced by Polyus research institute in Moscow [5], [6].

In particular, by changing the width of active region (Quantum Well), waveguide width, as well by changing the waveguide profile by introducing a gradual change of Al concentration, we were able to decrease significantly the lasing threshold current, increase the slope of optical power versus current, and increase optical efficiency [3].

We have shown also [4] that the lasing action may not occur at certain widths or depths of Quantum Well (QW), and the threshold current as a function of the width may have discontinuities. The effects are more pronounced at low temperatures. We argue that these discontinuities occur when the most upper quantum well energy values are very close to either conduction band or valence band energy offsets. The effects may be observed at certain conditions in temperature dependence of lasing threshold current as well.

The main challenges with the broader use of AlGaAs based SCH lasers are related to improving some of their electro-optical characteristics, in particular their optical efficiency.

The purpose of this work is to investigate the role of doping levels across the laser structure, and, if only possible, to find doping concentrations that would lead to the best opto-electrical parameters, maximizing optical effi-

ciency.

We assume here uniform doping profiles accross laser layers.

For simulations, we use Sentaurus TCAD from Synopsys [7], which is an advanced commercial computational environment, a collection of tools for performing modeling of electronic devices.

## 2 Lasers structure and callibration of modeling.

We model a laser with  $1000\mu m$  cavity length and  $100\mu m$  laser width, with doping/Al-content as described in Table 1. The table 2 describes its experimental parameters.

Synopsys's Sentaurus TCAD, used for modeling, can be run on Windows and Linux OS. Linux, once mastered, offers more ways of an efficient solving of problems by providing a large set of open source tools and ergonomic environment for their use, making it our preferred operating system. This is an advanced, flexible set of tools used for modeling a broad range of technological and physical processes in the world of microelectronics phenomena. In case of lasers, some calculations in Sentaurus have purely phenomenological nature. The electrical and optical characteristics depend, primarily, on the following computational parameters that are available for adjusting:

*AreaFactor* of electrodes,  $A_e$ , *AreaFactor* in Physics section,  $A_{ph}$ , electrical contact resistance  $R_x$ . There are several parameters for adjustment that are related to microscopic physical properties of materials or structures studied. However, often their values are either unknown exactly or finding them would require quantum-mechanical modeling of electronic band structure and transport, based on first-principles. This is however not the aim of our work.

In order to find agreement between the calculated results and these observed experimentaly (the threshold current  $I_{th}$  and the slope of Optical Power,  $S = dL/dI$ , are such most basic laser parameters), we adjust accordingly values of  $A_e$  and  $A_{ph}$ .

The results for  $I_{th}$  and  $S$ , in this paper, are all shown normalized by  $I_{th}^0$

and  $S_0$ , respectively, which are the values computed for the reference laser described in Table 1.

We neglect here the effect of contact resistance,  $R_x$ , by not including buffer and substrate layers and contacts into calculations (compare with structure described in Table 1). We use *InnerVoltage* parameter available in Sentaurus and treat it as a physical quantity that is closely related to voltage applied. Another parameter available in Sentaurus, *OuterVoltage*, is simply related to *InnerVoltage* by the ohmic formula:  $OuterVoltage = InnerVoltage + R_x \cdot I$ . Hence, any results shown here may be easily adjusted after calculations by adding the effect of  $R_x$ .

Let us estimate the value of  $R_x$ . We assume that this is the sum of electrical resistance of n-substrate, n-buffer, and p-contact layers (see Table 1). By using simplified formula for each of these layers,  $\rho = 1/(ne\mu)$ , and electron/hole mobility from database of Synopsys, we have the following specific resistivity values for these layers (indexed as rows in Table 1):  $\rho_1 = \frac{1}{2720} \frac{cmV}{A}$ ,  $\rho_2 = \frac{1}{1360} \frac{cmV}{A}$ , and  $\rho_8 = \frac{1}{2560} \frac{cmV}{A}$ . Taking into account appropriate geometrical dimensions, we obtain:  $r_1 = 0.013\Omega$ ,  $r_2 = 3 \cdot 10^{-5}\Omega$ , and  $r_8 = 3 \cdot 10^{-5}\Omega$ . Hence,  $R_x$  is dominated by the resistance of n-substrate layer and it is of the order of  $R_x = 13m\Omega$ . At threshold current of  $0.1A$ , that small resistance will cause a difference between computed by us lasing offset voltage  $U_0$  and that one measured by about  $1mV$  only. It will however have a noticeable contribution to differential resistance  $dU/dI$ .

Table 1: Structure of AlGaAs SCH laser layers used in computer modeling.

No	Layer	Composition	Doping [ $cm^{-3}$ ]	Thickness [ $\mu m$ ]
1	n-substrate	n-GaAs (100)	$2 \cdot 10^{18}$	350
2	n-buffer	n-GaAs	$1 \cdot 10^{18}$	0.4
3	n-emitter	$Al_{0.5}Ga_{0.5}As$	$1 \cdot 10^{18}$	1.6
4	waveguide	$Al_{0.33}Ga_{0.67}As$	none ( $n \approx 10^{15}$ )	0.2
5	active region (QW)	$Al_{0.08}Ga_{0.92}As$	none ( $n \approx 10^{15}$ )	0.012
6	waveguide	$Al_{0.33}Ga_{0.67}As$	none ( $n \approx 10^{15}$ )	0.2
7	p-emitter	$Al_{0.5}Ga_{0.5}As$	$1 \cdot 10^{18}$	1.6
8	contact layer	p-GaAs	$4 \cdot 10^{19}$	0.5

Table 2: Summary of experimental conditions and laser parameters.

Temperature [K]	300
Lasing wavelength [nm]	808
Offset voltage $U_0$ [V]	1.56-1.60
Differential resistance, $r = dU/dI$ [ $m\Omega$ ]	50-80
Threshold current $I_{th}$ [mA]	200-300
Slope of optical power, $S = dL/dI$ [W/A]	1.15-1.25
Left mirror reflection coefficient $R_l$	0.05
Right mirror reflection coefficient $R_r$	0.95

## 3 Methods of data analysis.

### 3.1 Using Perl, TCL, gnuplot, and other open source tools on Linux.

It is possible to work in a batch mode in Sentaurus TCAD. However, we find it more convenient to use Perl<sup>1</sup> scripts rather for control of batch processing and changing parameters of calculations. It is a very flexible programming language, suitable in particular for working on text files (e.g. manipulation on text data files), and it is convenient to be used from terminal window rather, not by using a GUI interface, which is a more productive approach towards computation.

Tcl<sup>2</sup> is a very powerful but easy to learn dynamic programming language, suitable for a wide range of uses. Sentaurus TCAD contains libraries designed to be used together with TCL. They are run through Sentaurus's tdx interface and are used for manipulating (extracting) spacial data from binary TDR files.

Besides, we use tools/programs like gnuplot, grep, shell commands, etc. A more detailed description, with examples of scripts, is available on our laboratory web site<sup>3</sup>.

### 3.2 Threshold current and $L(I)$ dependence.

The most accurate way of finding  $I_{th}$  is by extrapolating the linear part of  $L(I)$  to  $L = 0$  just after the current larger than  $I_{th}$ . We used a set of gnuplot and perl scripts for that that could be run semi-automatically on a large collection of data. One should only take care here that a properly chosen is the data range for fitting, since  $L(I)$  is a linear function in a certain range of  $I$  values only. The choice of that range may affect accuracy of data analysis. We find however that this is the most accurate effective method to analyse the data from a large collection of datasets.

---

<sup>1</sup>Perl stands for *Practical Extraction and Report Language*; <http://www.perl.org>

<sup>2</sup>*Tool Command Language*; <http://www.tcl.tk>

<sup>3</sup><http://www.ostu.ru/units/ltd/zbigniew/synopsys.php>

### 3.3 Three ways of finding lasing offset voltage $U_0$ .

#### 3.3.1 $U_0$ from fitting $U(I)$ dependence

Textbooks' exponential  $U(I)$  dependence is fulfilled well at voltages which are well below the lasing offset voltage  $U_0$ . Near the lasing threshold, we observe a strong departure from that dependence, and, in particular, for many data curves a clear kink in  $U(I)$  is observed at  $U_0$ . We find that a modified exponential dependence describes the data very well:

$$\begin{aligned} I(U) &= I_{th} \cdot \exp(B \cdot (U - U_0) + C \cdot (U - U_0)^2), \quad \text{for } U < U_0 \\ I(U) &= I_{th} \cdot \exp(D \cdot (U - U_0) + E \cdot (U - U_0)^2), \quad \text{for } U > U_0 \end{aligned} \quad (1)$$

where  $I_{th}$ ,  $U_0$ , as well  $B$ ,  $C$ ,  $D$ , and  $E$  are certain fitting parameters.

The above function is continuous at  $U_0$ , as it obviously should, but its derivative is usually not. We used Equation (1) to find out  $I_{th}$  and  $U_0$ . However, the accuracy of this method was found lower than accuracy of the following two methods described. Figure 1 shows a few typical examples of  $I(U)$  dependencies, together with lines computed to fit them by using (1).

Let us notice that since (1) may have a discontinuous derivative, using it to find out differential resistance at  $U_0$  is ambiguous. From Equation (1), at  $U = U_0$ , we will have  $dU/dI = \frac{1}{I_{th} \cdot B}$  on the side  $U < U_0$  and  $dU/dI = \frac{1}{I_{th} \cdot D}$  on the side  $U > U_0$ .

In fact, the differential resistance measured in experiments is, to some extent, determined by the resistance of buffer layers and contacts, and by the way how it has been actually defined for non-linear  $I - V$  curves.

In practice, the  $U(I)$  dependence, above  $U_0$  but not far above, may be assumed to be a linear function. In such a case, we find from data analysis, for the third dataset, for instance, in Figure 1,  $dU/dI \approx 50m\Omega$ , which, together with computed contact resistance  $R_x = 13m\Omega$  gives good qualitative agreement with the differential resistance expected for real laser, as listed in Table 2.



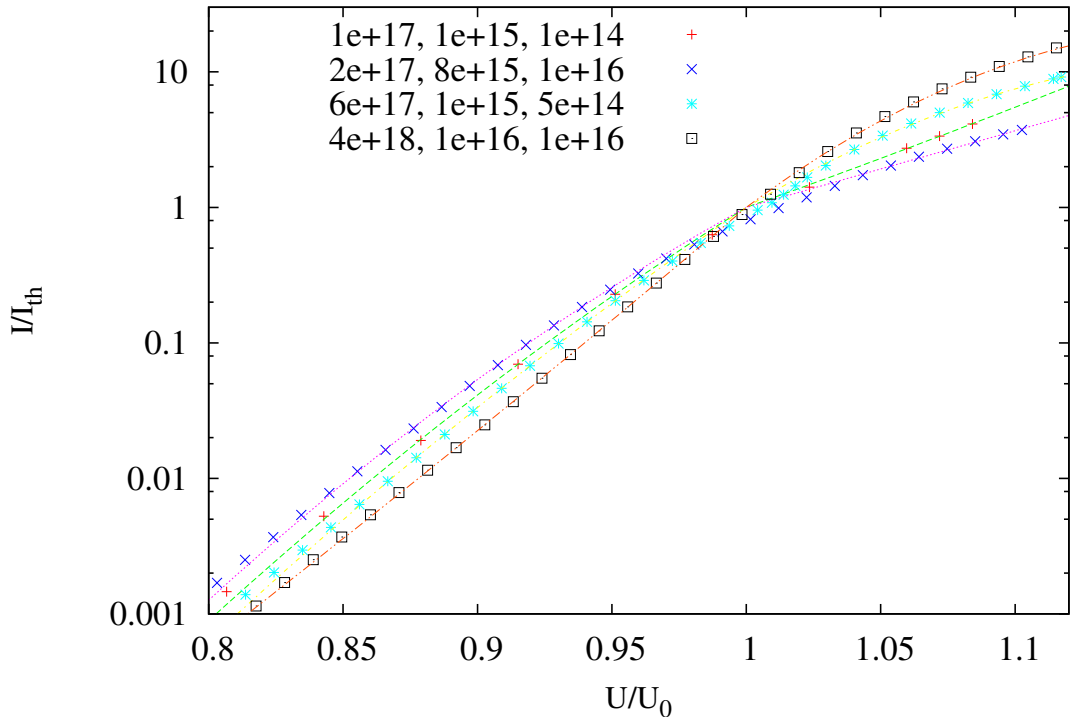


Figure 1: Examples of typical  $I - V$  characteristics for a few combination (as described in the Figure) of doping concentrations (n- and p-emitters concentration first, followed by waveguides and active region concentrations). We show the narrow region near the lasing threshold, only. The curves are computed by using fitting parameters ( $I_{th}, B, C, D, E, U_0$ ) of equation (1), and after that voltage is normalized by  $U_0$  and current by  $I_{th}$ .

### 3.3.2 $U_0$ from maximum of $d \log L(U)/dU$ .

Another approach to find  $U_0$  is by finding position of maximum in derivative of logarithm of  $L$  versus voltage:  $dL(U)/(LdU)$ . This is a very accurate method when there is a sufficiently large number of datapoints available near  $U_0$ . However, for that, we would have to perform a lot of computations that are time consuming, in small enough steps in  $U$ . Hence, this method is not always effective.

### 3.3.3 $U_0$ from gain versus voltage curves.

We find that a good accuracy of determining  $U_0$  is from extrapolating linearly gain versus voltage curve in a near range of voltage values below  $U_0$ , to the value of maximal gain, which is constant above  $U_0$ . The results presented in this paper were obtained that way.

### 3.4 Differential resistance and optical efficiency.

Let us use the simplified assumption that  $U(I)$  is linear above  $U_0$ :  $U(I) = U_0 + r \cdot (I - I_{th})$ . Together with linear dependence of lasing light power versus current,  $L = S \cdot (I - I_{th})$ , we have the following relation between optical power efficiency,  $\eta = L/P$ , and current  $i = (I - I_{th})/I_{th}$ :

$$\eta = \frac{S}{U_0} \cdot \frac{i}{\left(1 + \frac{r \cdot I_{th}}{U_0} \cdot i\right)^{(1+i)}} \quad (2)$$

Equation 2 gives a reasonably accurate qualitative description of  $\eta(i)$ . The parameter determining position and value of maximum,  $\eta_{max}(i_{max})$ , is governed by factor  $\alpha = \frac{r \cdot I_{th}}{U_0}$ . In a typical case, with  $r = 60m\Omega$ ,  $U_0 = 1.65V$ , and  $I_{th} = 0.2A$ , we have  $\alpha \approx 7 \cdot 10^{-3}$ .

We sometime prefer to use another form of Equation 2, where  $\eta$  as a function of voltage is used:

$$\eta = \frac{S}{U_0} \cdot \frac{u-1}{u \cdot \left(u + \frac{r \cdot I_{th}}{U_0} - 1\right)} \quad (3)$$

where  $u = U/U_0$ .

Figure 2 shows a few examples of  $\eta(U)$  curves computed with Equation 3.

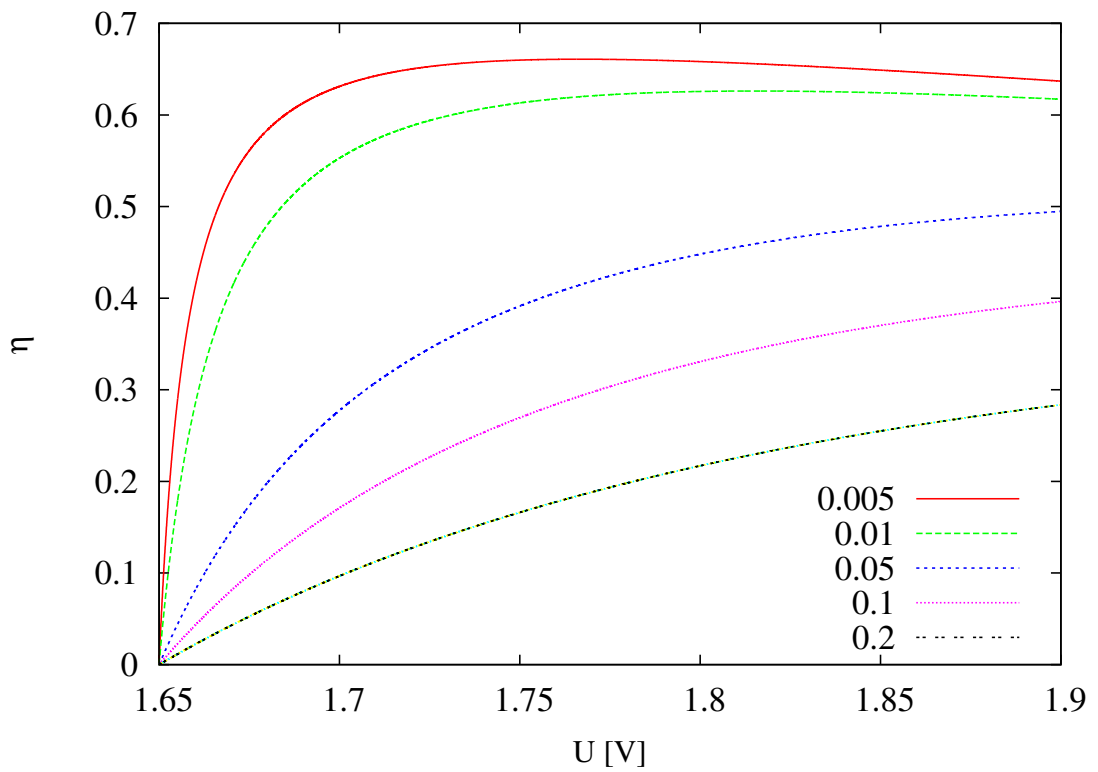


Figure 2: Optical efficiency as a function of voltage, computed by using Equation 3, for a few values of parameter  $\alpha = \frac{r \cdot J_{th}}{U_0}$ , as shown in the Figure. It has been assumed that  $S = 1.25W/A$  and  $U_0 = 1.65V$ .

## 4 N-N waweguide structure.

By "N-N" waveguide structure we mean a doping structure as described in Table 1, where both waveguides and the active region (QW) are n-type doped.

We present here selected examples only of data obtained from semi-automatic analyses of thousands of datasets.

### 4.1 The role of doping in Active Region (QW).

Figures 3, 4, and 5 show the role of doping concentration in active region, for a few values of doping concentrations in emitter regions, on basic characteristics of lasers: threshold current, slope of light power versus current,  $dL(I)/dI$ , and lasing offset voltage, respectively. The doping concentration in waveguide regions is the same on these three figures; it is  $10^{15}/cm^3$ .

We see that none of these quantities, i.e.  $I_{th}$ ,  $dL/dI$ ,  $U_0$ , depends strongly on active region doping.

Therefore, it is not unexpected that the optical efficiency, the ratio of optical power  $L$  to total power supplied to the laser,  $P = U \cdot I$ , as shown in Figure 6, weakly depends on doping concentration in active region as well. Though for the lower doping the higher optical efficiency is obtained.

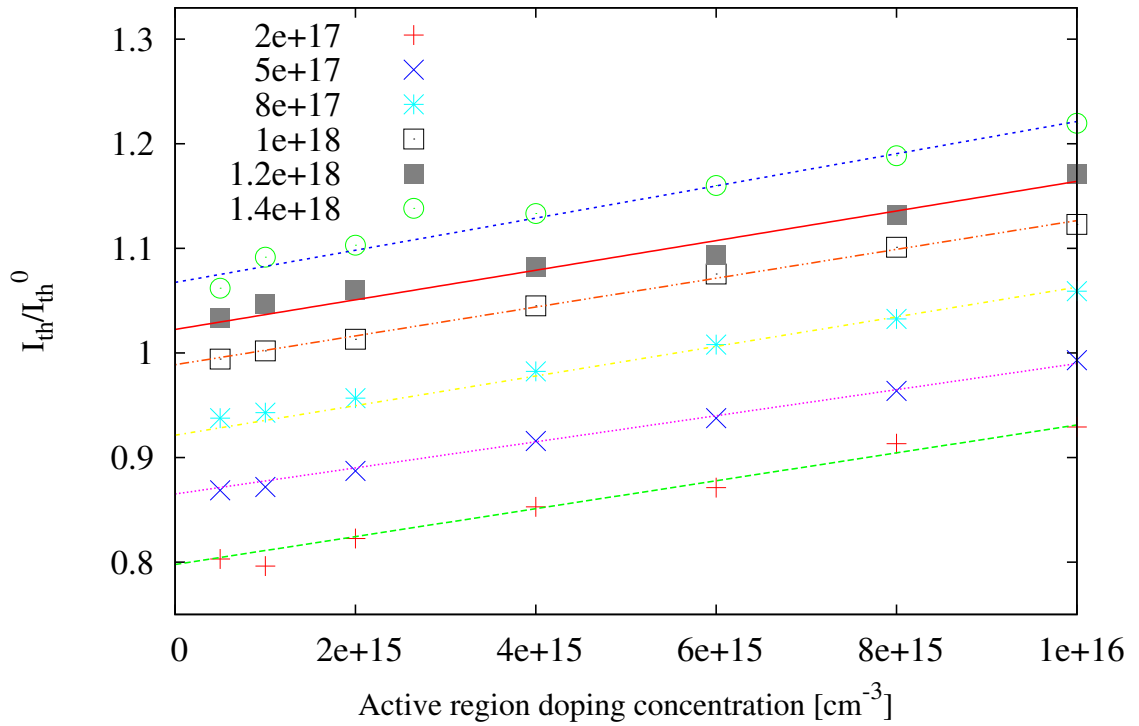


Figure 3: Threshold current,  $I_{th}$ , normalized by  $I_{th}^0$ , as a function of doping concentration in active region, for a range of doping concentrations in emitter regions, as indicated in the figure. Doping concentration in waveguide regions is kept constant at value of  $10^{15}/\text{cm}^3$ .

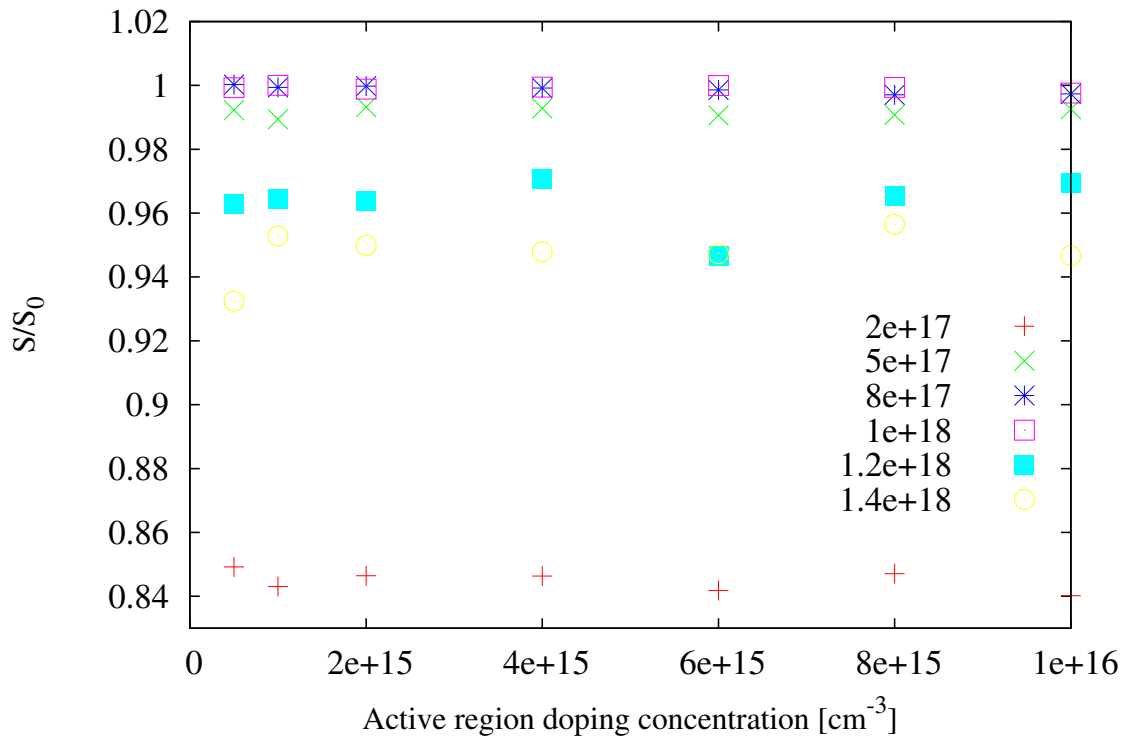


Figure 4:  $S$  normalized by  $S_0$ , as a function of doping concentration in active region, for a range of doping concentrations in emitter regions, as indicated in the figure. Doping concentration in waveguide regions is kept constant at value of  $10^{15}/\text{cm}^3$ . These data correspond to datapoints displayed for  $I_{th}$  in Figure 3.

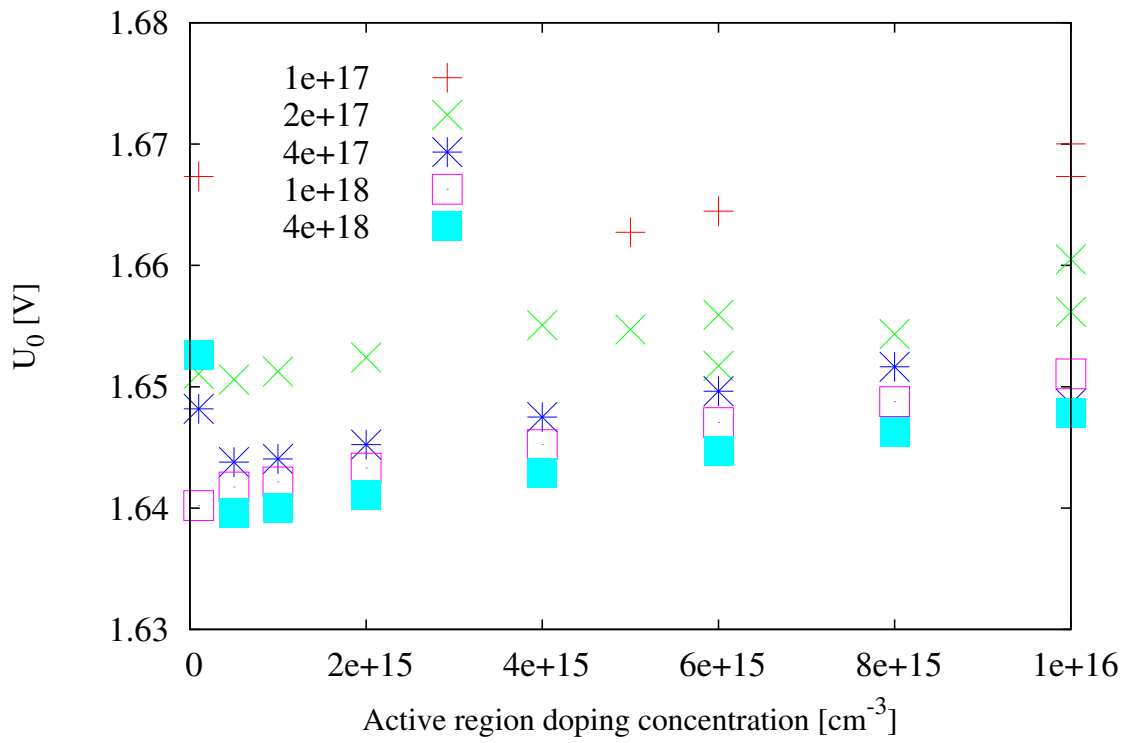


Figure 5:  $U_0$  as a function of doping concentration in active region, for a range of doping concentrations in emitter regions, as indicated in the figure. Doping concentration in waveguide regions is kept constant at value of  $10^{15}/\text{cm}^3$ . These data correspond to datapoints displayed for  $I_{th}$  in Figure 3.

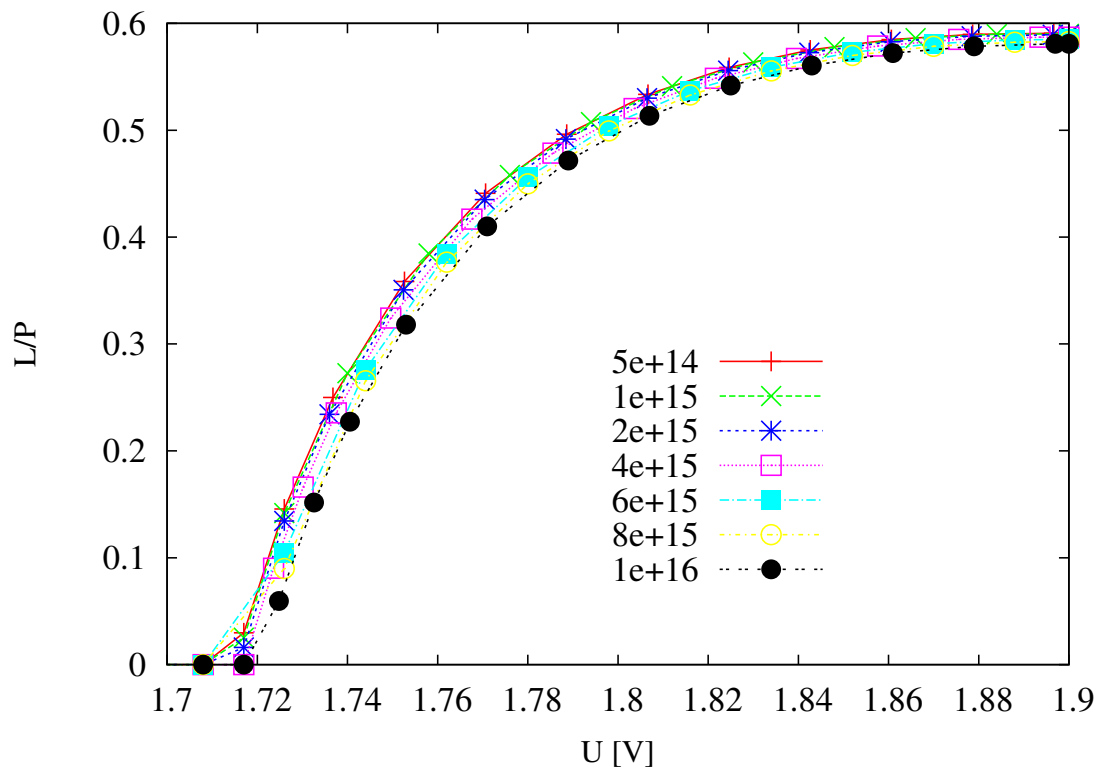


Figure 6: Optical efficiency versus applied voltage, for a few values of doping concentration in active region, as described in the Figure. Doping concentrations in waveguide regions is  $10^{15}/cm^3$ , and in emitters regions it is  $10^{18}/cm^3$ .



## 4.2 The role of doping in Waveguide Regions.

The effects of doping in waveguide regions are similar to these in the active region, but stronger.

Figures 7, 8, 9, and 10 illustrate, respectively, dependencies of threshold current,  $dL/dI$ , lasing offset voltage  $U_0$ , and optical efficiency on doping levels in waveguide regions. We observe, again, that the best characteristics (lowest  $I_{th}$  and highest  $dL/dI$  values) are at lowest doping levels in waveguides.  $U_0$  also weakly depends on doping in waveguides. The most significant role is played by doping in emitters regions, rather. However, as Figure 10 shows, optical efficiency changes significantly with doping levels. One would like here to use Equation 3 to describe the data in this Figure. However, it could provide only a very qualitative fitting of the data. Since all the data in this figure indicate on the same or very close values of  $U_0$  (compare also results of Figure 9), we attribute large differences between these curves to significant increase of differential resistance  $r = dU/dI$  when doping level increases. And that could be understood as building up of p-n junction outside of quantum well region, with increase of doping.

A characteristic for "N-N" structure is parabolic dependence of optical efficiency on doping levels, as shown in Figure 11.

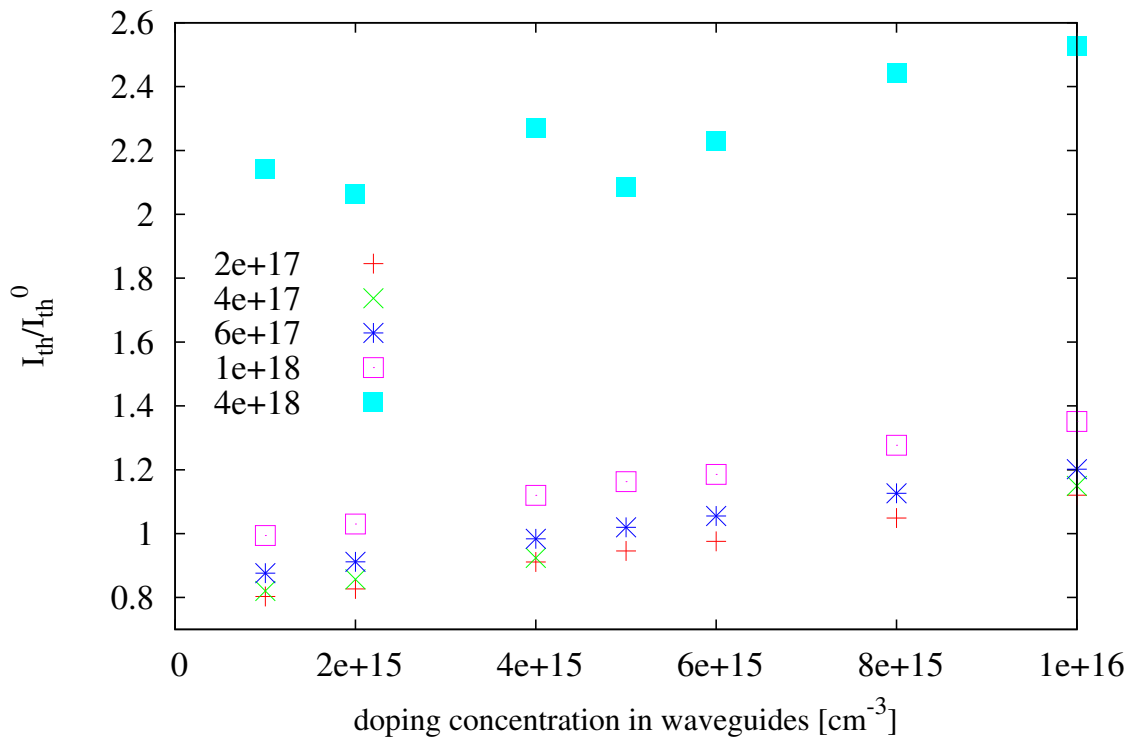


Figure 7: Threshold current  $I_{th}$ , normalized by  $I_{th}^0$ , as a function of doping concentration in waveguide regions, when doping concentration in active region is  $5 \cdot 10^{14}/\text{cm}^3$ , for several values of doping concentration in n- and p-emitters, as shown in the Figure.

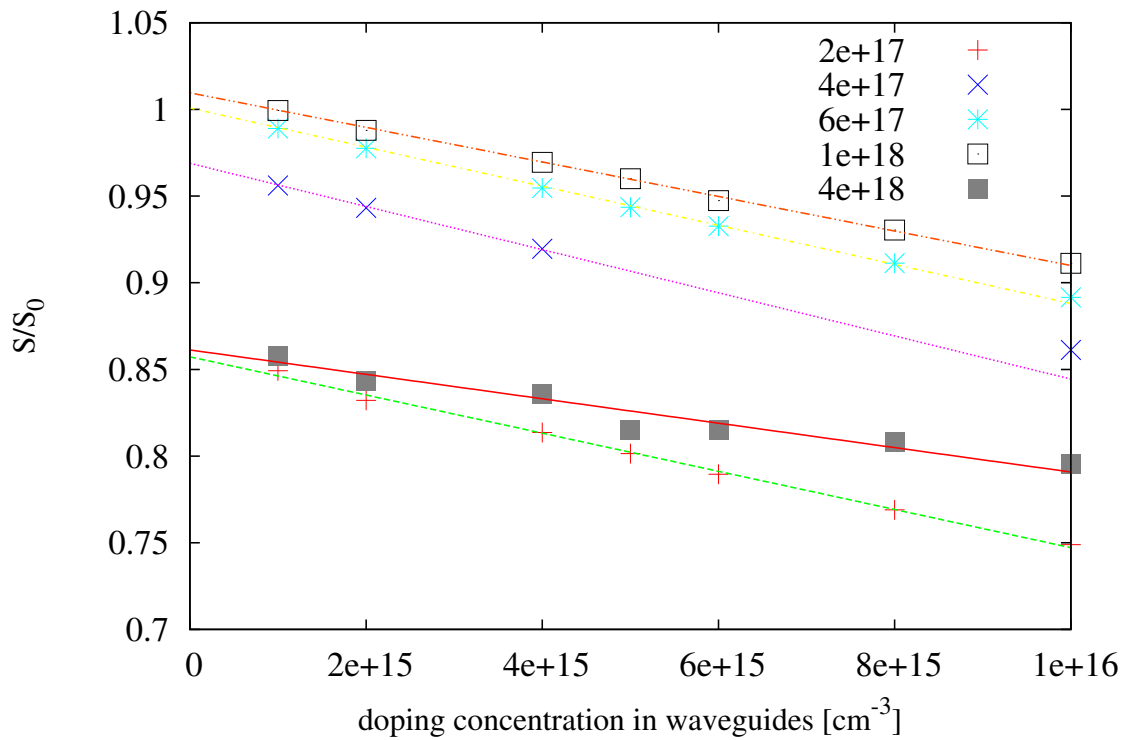


Figure 8: The slope  $S = dL/dI$ , normalized by  $S_0$ , as a function of doping concentration in waveguide regions, when doping concentration in active region is  $5 \cdot 10^{14}/\text{cm}^3$ , for several values of doping concentration in n- and p-emitters, as shown in the Figure.

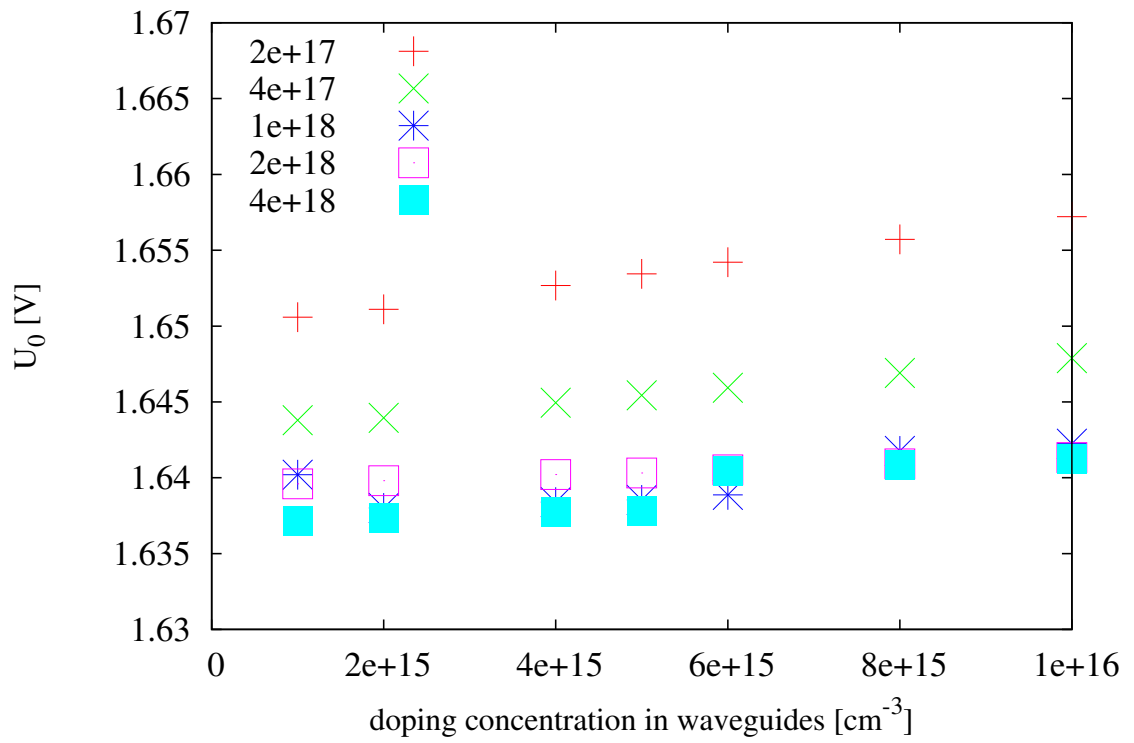


Figure 9: Lasing offset voltage  $U_0$ , as a function of doping concentration in waveguide regions, when doping concentration in active region is  $5 \cdot 10^{14}/\text{cm}^3$ , for several values of doping concentrations in n- and p-emitters, as shown in the Figure.

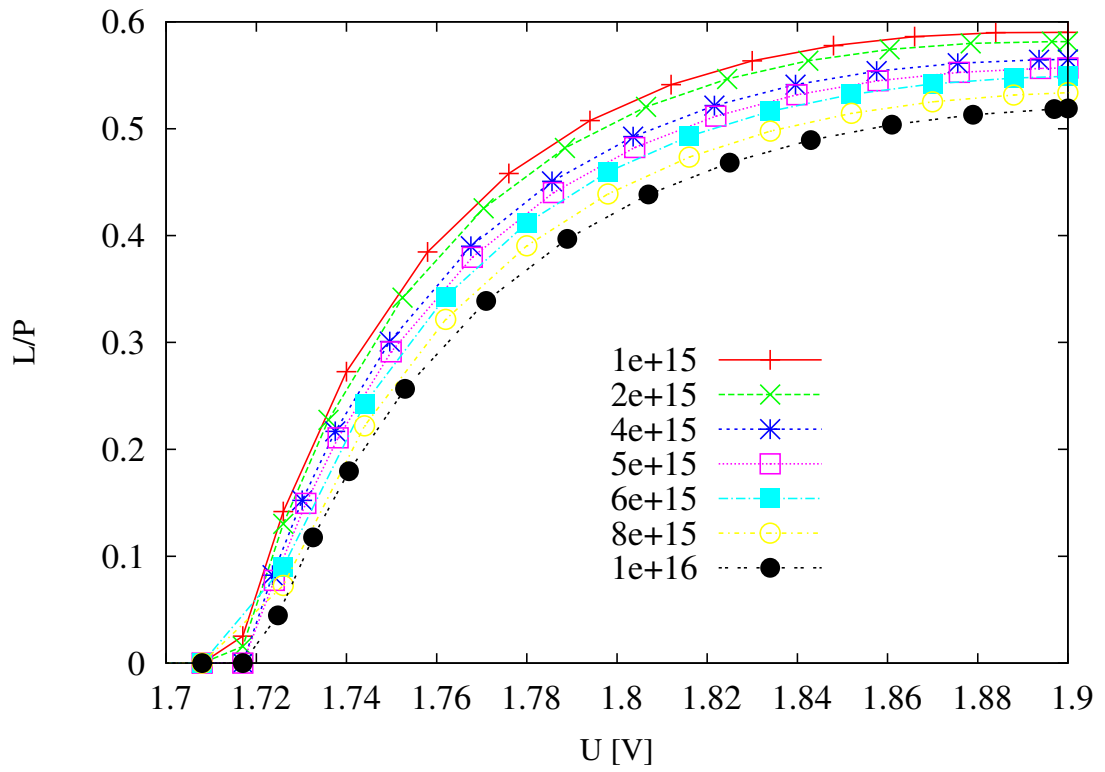


Figure 10: Optical efficiency versus applied voltage, for a few values of doping concentration in waveguide region, as described in the Figure. Doping concentrations in active region is  $10^{15}/cm^3$ , and in emitters regions it is  $10^{18}/cm^3$ .

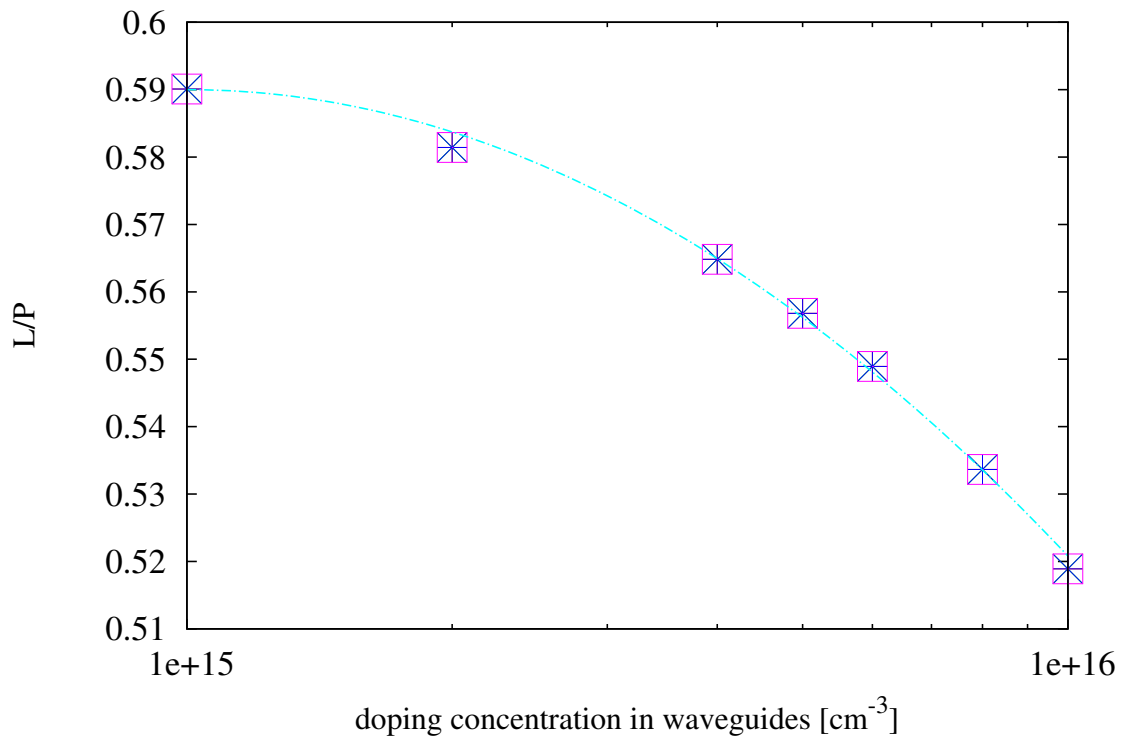


Figure 11: Optical efficiency at applied voltage of  $1.9V$ , as a function of doping concentration in waveguide regions, when doping concentrations in active regions is  $10^{15}/\text{cm}^3$ , and in emitters regions it is  $10^{18}/\text{cm}^3$ . Notice logarithmic scale on x-axes. The solid curve is a least-squares fitting of the function  $L/P = A \cdot (\log(x/x_0))^2 + B$ , where  $A = 0.01305$ ,  $x_0 = 1.0 \cdot 10^{15}$ , and  $B = 0.590$ .

### 4.3 The role of doping in Emitters Regions.

Doping levels in emitters regions contribute in the most prominent degree to laser characteristics.

Figures 12 and 13 show typical example dependencies of  $I_{th}$  and  $dL/dI$  on doping in emitters. Clearly is observed a minimum in  $I_{th}(d_e)$  at  $d_e$  somewhat lower than  $10^{18}cm^{-3}$ , and a maximum in  $S(d_e)$  at a value of  $d_e$  close to that but not the same.

In Figures 14, 15 and 16, we show the presence of such a minimum in  $I_{th}(d_e)$  for a few more sets of data. We show that a parabolic dependence (when doping concentration is drawn on logarithmic axes) is a good approximation of the data: compare the same results as in Figure 15 shown however in linear scale in Figure 16:

$$I_{th}(d_e) = I_0 + a \cdot \log \left( \frac{d_e}{x_0} \right)^2, \quad (4)$$

where  $I_0$ ,  $a$ , and  $x_0$  are certain fitting parameters.

The lasing offset voltage  $U_0$  (Figures 17 and 18) is sensitive to emitters doping at low levels, only, below around  $10^{18}cm^{-3}$ .

Strong dependencies of  $I_{th}$  and  $dL/dI$  on doping manifest itself in a strong dependence of optical efficiency on doping levels, as Figure 19 shows. Again, it has a parabolic character (Figure 19), similar to that one found for waveguides (Figure 11).

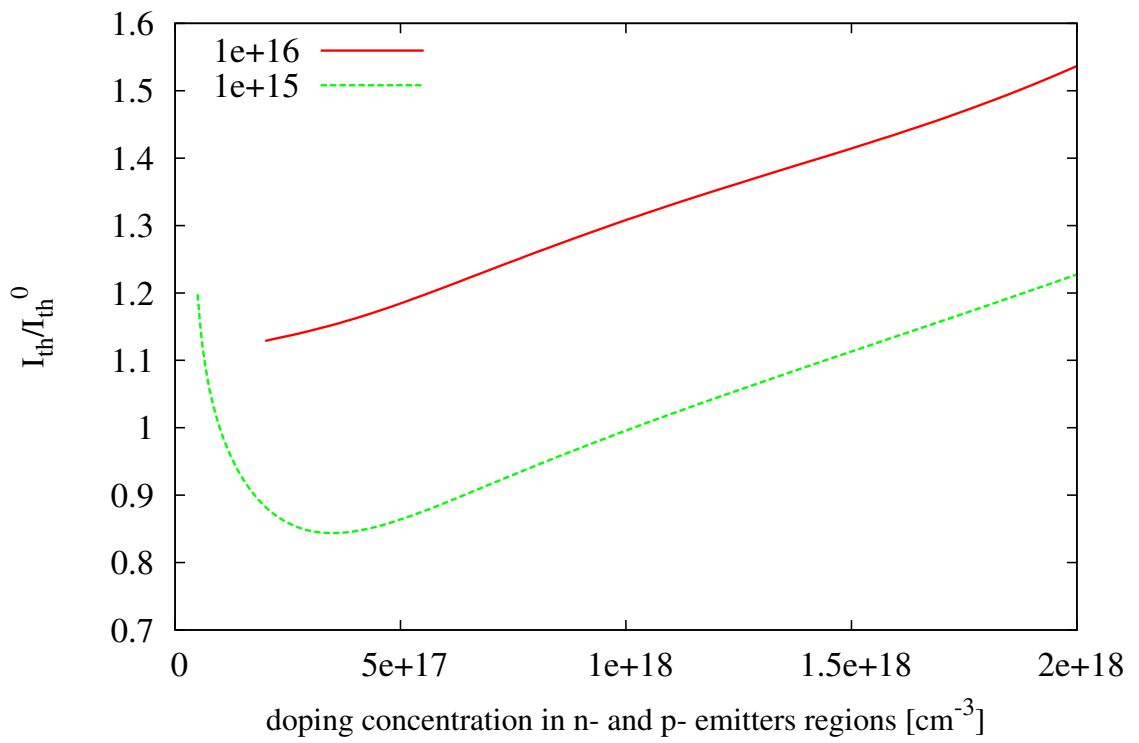


Figure 12: Threshold current,  $I_{th}$ , normalized by  $I_{th}^0$ , as a function of doping concentration in n- and p-emitters, when doping concentration in active region is  $10^{15}/cm^3$  and in waveguide  $10^{15}/cm^3$  and  $10^{16}/cm^3$ .



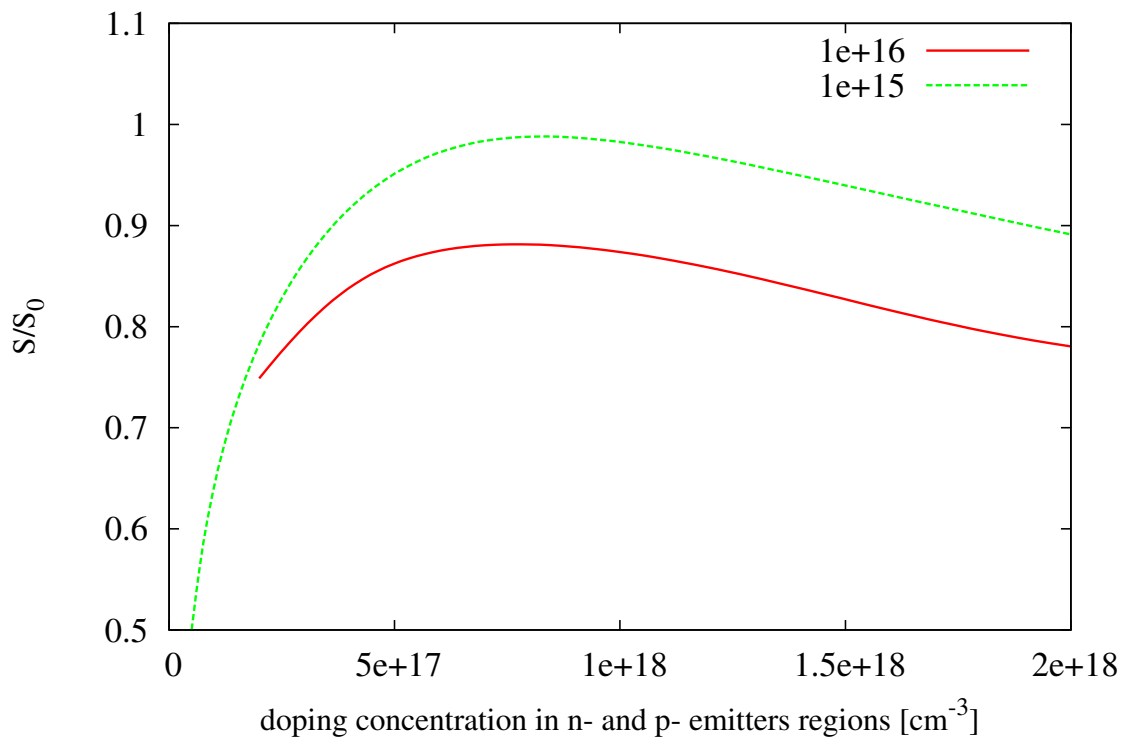


Figure 13: The slope  $S = dL/dI$ , normalized by  $S_0$ , as a function of doping concentration in n- and p-emitters, when doping concentration in active region is  $10^{15}/\text{cm}^3$  and in waveguide  $10^{15}/\text{cm}^3$  and  $10^{16}/\text{cm}^3$ .

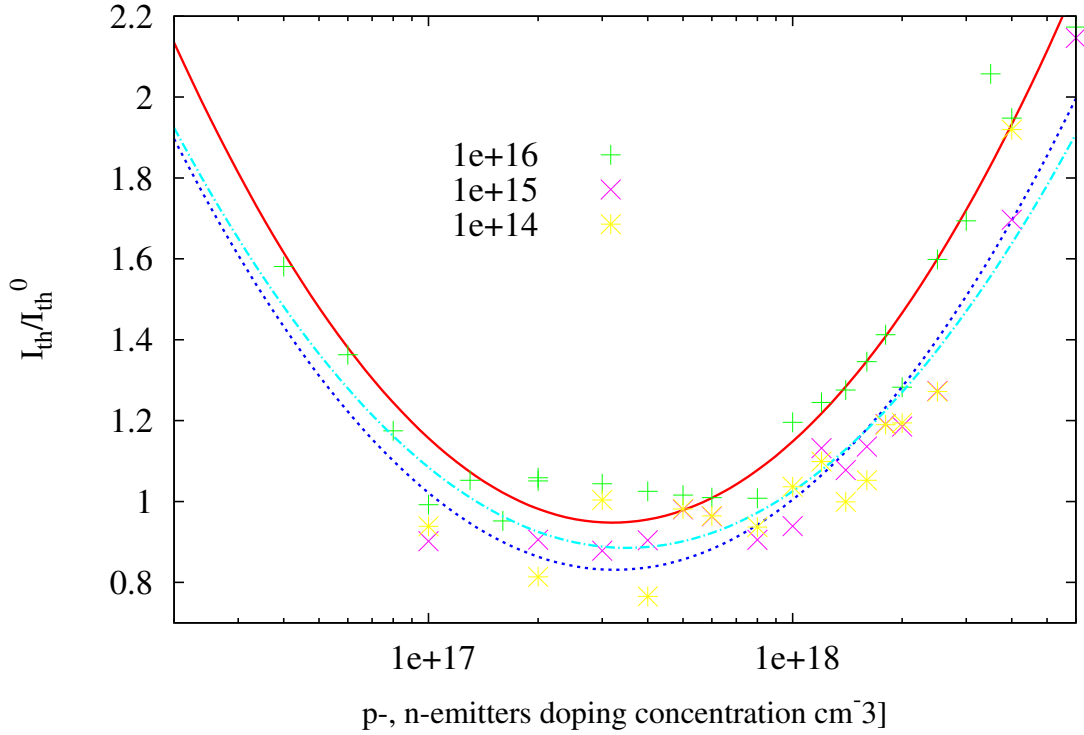


Figure 14: Normalized threshold current as a function of n- and p-emitters doping concentration, for a few values of doping concentrations in active region, as indicated in the Figure. Doping concentration in waveguide is  $10^{15}/\text{cm}^3$ . The lines are drawn by using least-squares fitting of the data according to equation:  $I_{th}(x) = I_0 + a \cdot (\log(x/x_0))^2$ , where  $I_0$ ,  $a$ , and  $x_0$  are certain fitting parameters. In this case, for active region doping concentration of  $10^{16}/\text{cm}^{-3}$ , the parameters values are:  $I_0 = 0.948$ ,  $a = 0.154$ ,  $x_0 = 3.2e + 17$ . When active region is  $10^{15}/\text{cm}^{-3}$ , the parameters values are:  $I_0 = 0.831$ ,  $a = 0.137$ ,  $x_0 = 3.25e + 17$ . When active region is  $10^{14}/\text{cm}^{-3}$ , the parameters values are:  $I_0 = 0.885$ ,  $a = 0.127$ ,  $x_0 = 3.5e + 17$ .

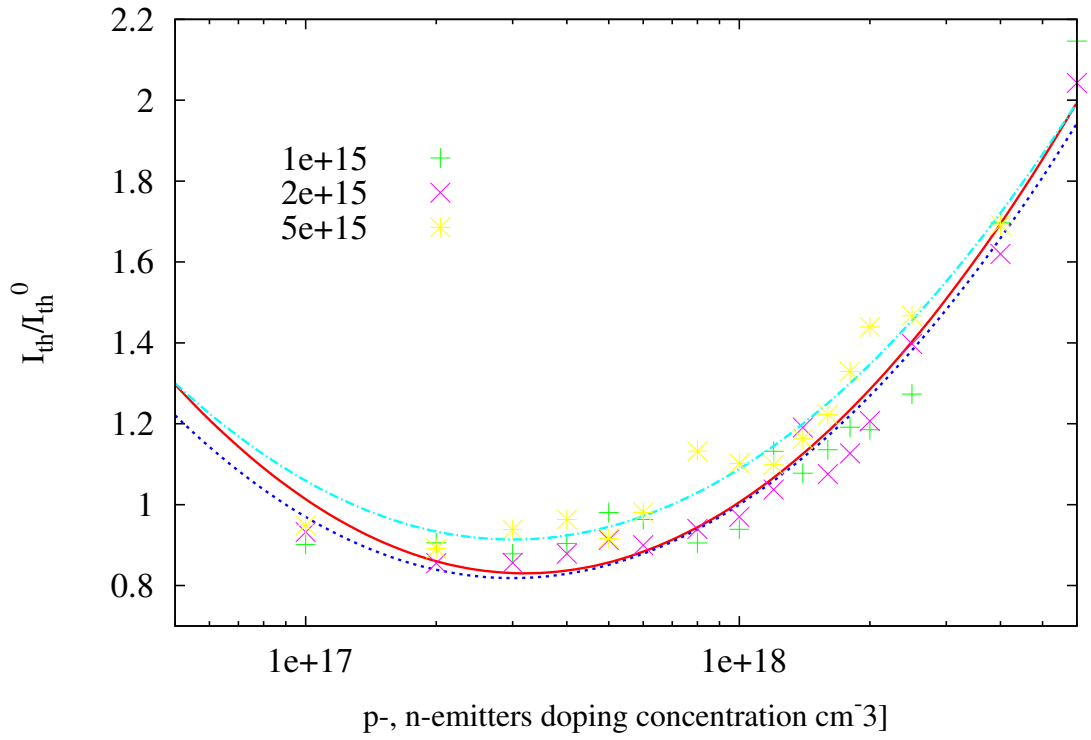


Figure 15: Normalized threshold current as a function of n- and p-emitters doping concentration, for a few values of doping concentrations in waveguide regions, as indicated in the Figure. Doping concentration in active region is  $10^{15}/cm^3$ . The lines are drawn by using least-squares fitting of the data according to equation:  $I_{th}(x) = I_0 + a \cdot (\log(x/x_0))^2$ , where  $I_0$ ,  $a$ , and  $x_0$  are certain fitting parameters.

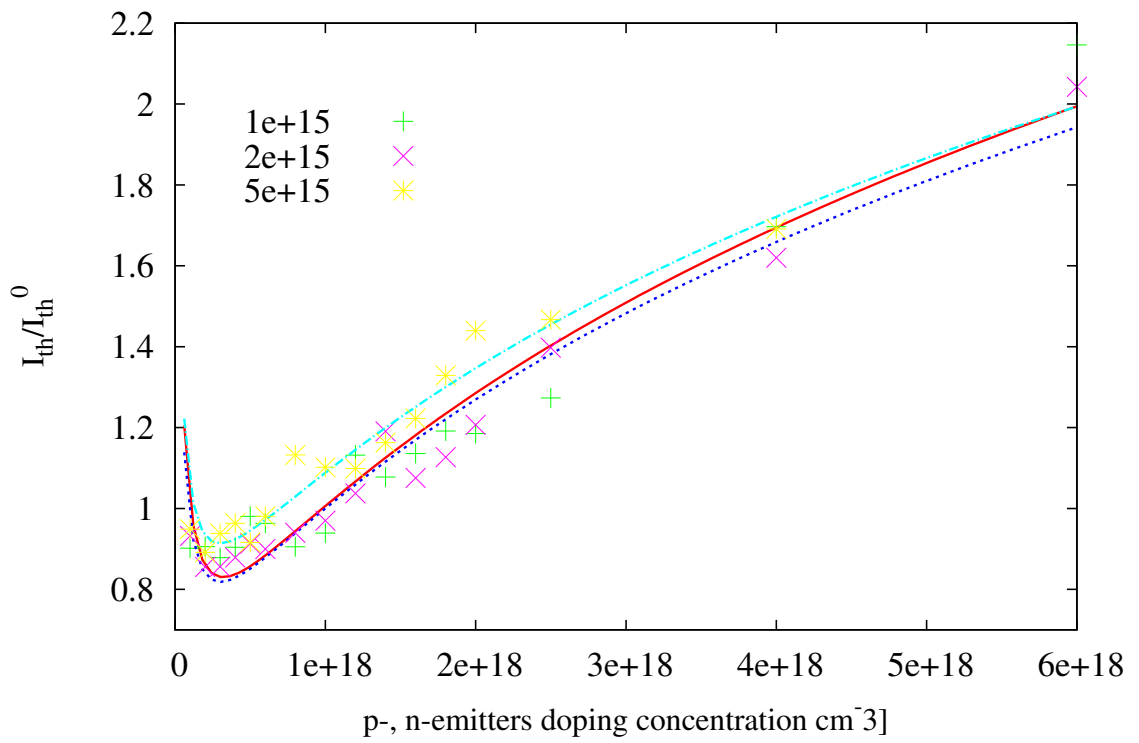


Figure 16: The same data and lines as in Figure 15, except the n- and p-emitters doping concentration axis is linear this time.

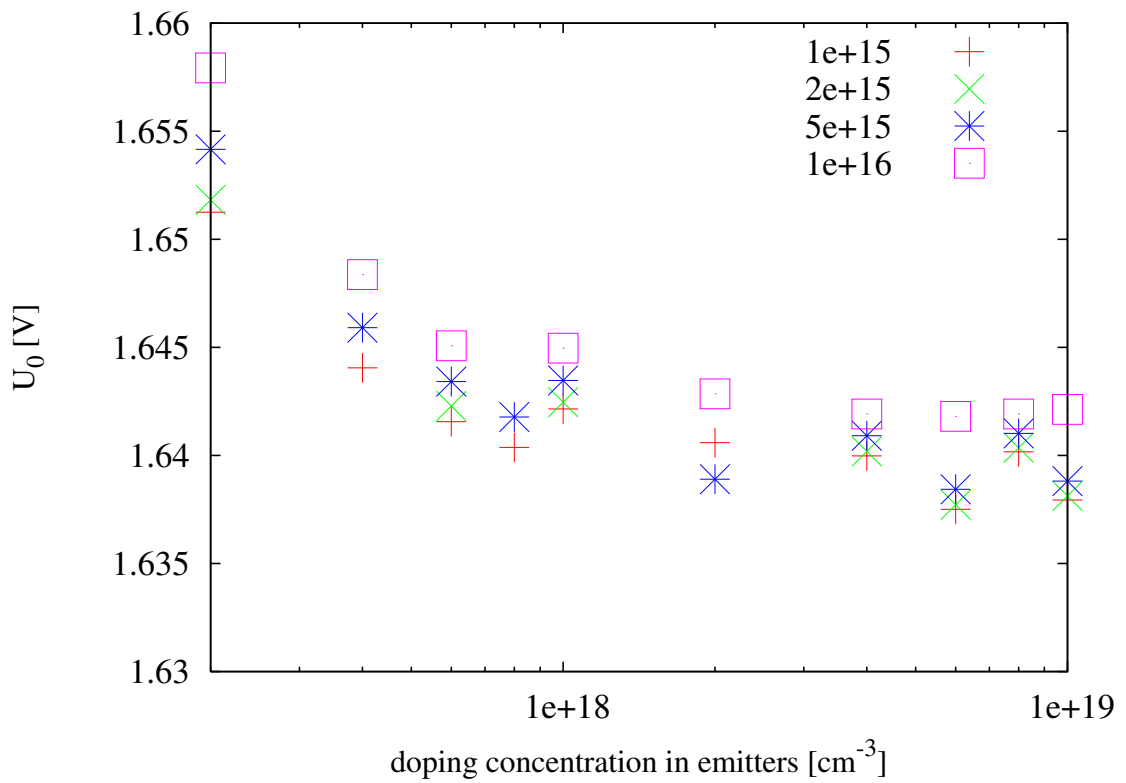


Figure 17:  $U_0$  as a function of n- and p-emitters doping concentration, for a few values of doping concentrations in waveguide regions, as indicated in the Figure. Doping concentration in active region is  $10^{15}/\text{cm}^3$ .

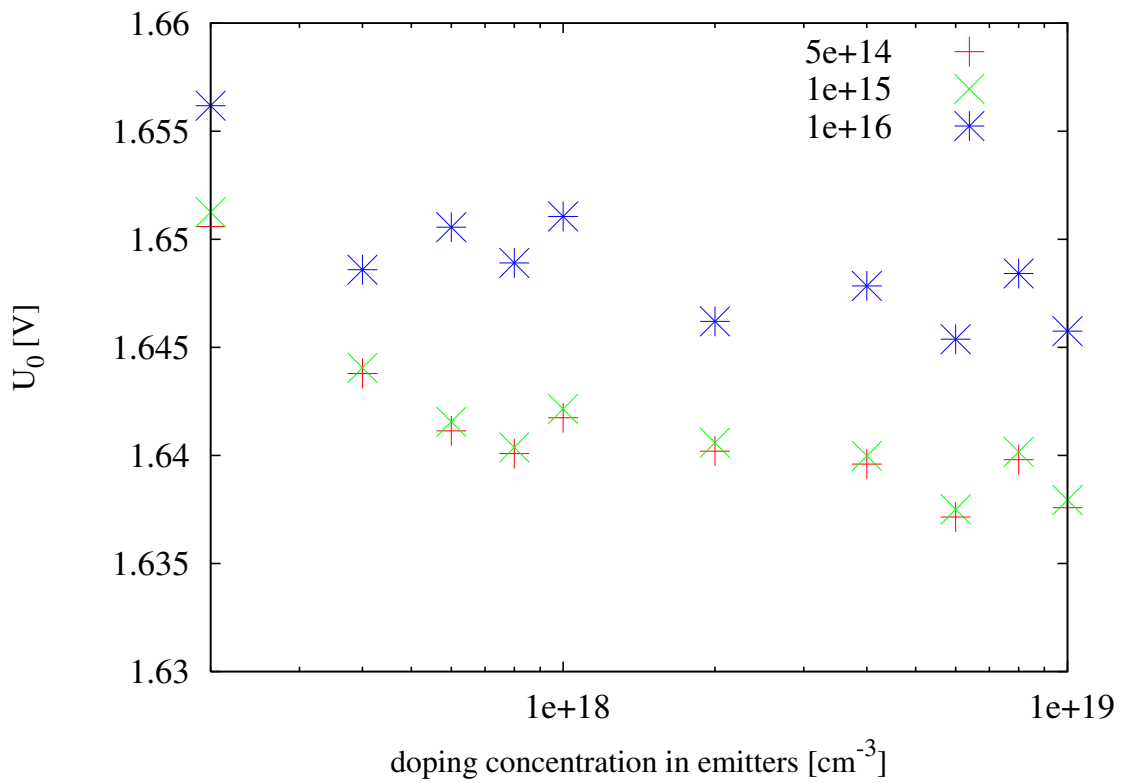


Figure 18:  $U_0$  as a function of n- and p-emitters doping concentration, for a few values of doping concentrations in active region, as indicated in the Figure. Doping concentration in waveguide regions is  $10^{15}/\text{cm}^3$ .

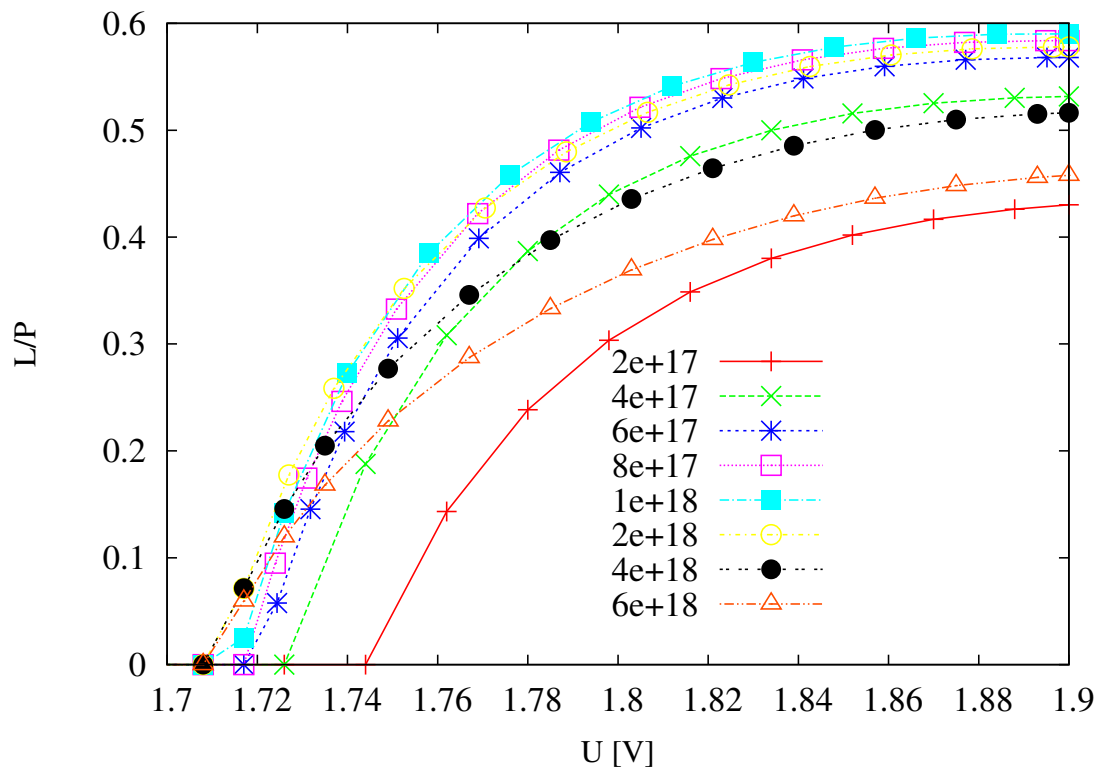


Figure 19: Optical efficiency versus applied voltage, for a few values of n- and p-emitters doping concentration, as described in the Figure. Doping concentrations in active region and waveguide regions is  $10^{15}/\text{cm}^3$ .

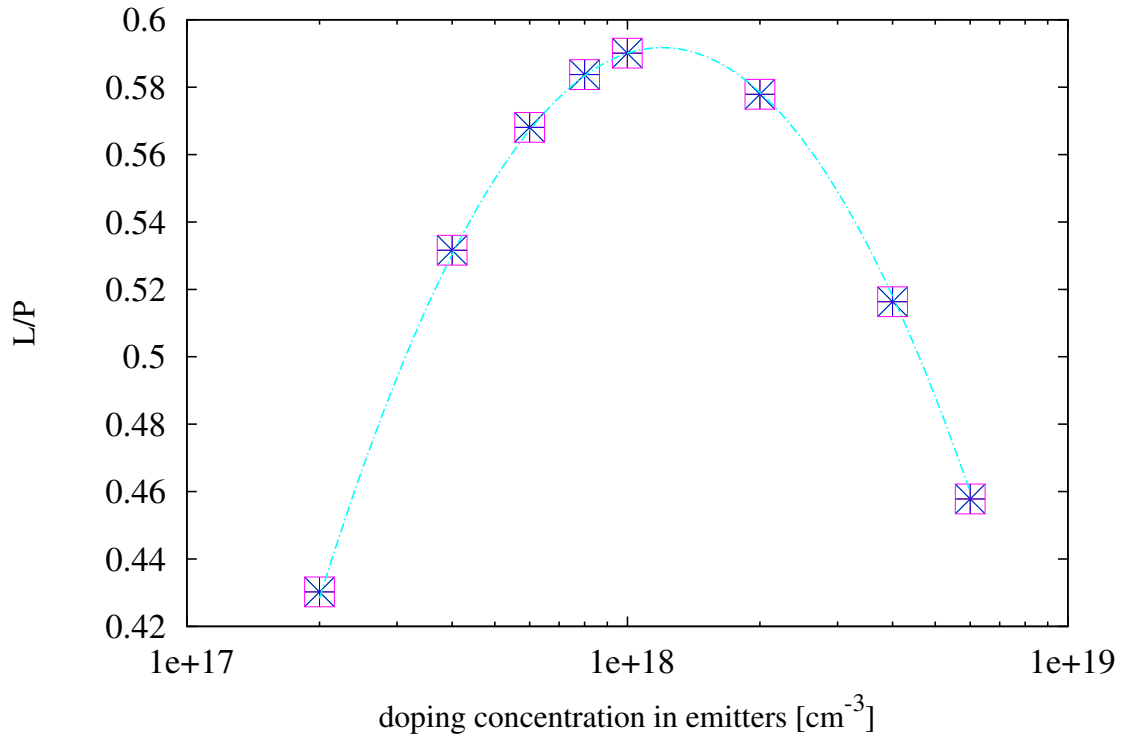


Figure 20: Optical efficiency at applied voltage of  $1.9V$ , as a function of doping concentration in emitters regions, when doping concentrations in waveguide and active regions is  $10^{15}/\text{cm}^3$ . The solid curve is a least-squares fitting of the function  $L/P = A \cdot (\log(x/x_0))^2 + B$ , where  $A = 0.0509$ ,  $x_0 = 1.2 \cdot 10^{18}$ , and  $B = 0.5917$ .



## 5 N-P waveguide structure.

By "N-P" waveguide structure we mean a doping structure that differs from that described in Table 1, where both waveguides and the active region (QW) are n-type doped. Here we assume that the waveguide on the side of n-emitter is of n-type, the other one is of p-type, and QW doping is of n-type.

The most remarkable difference between N-N and N-P structures is that in case of the last one a large reduction of  $I_{th}$  and a significant increase in  $dL/dI$  and in optical efficiency are found.

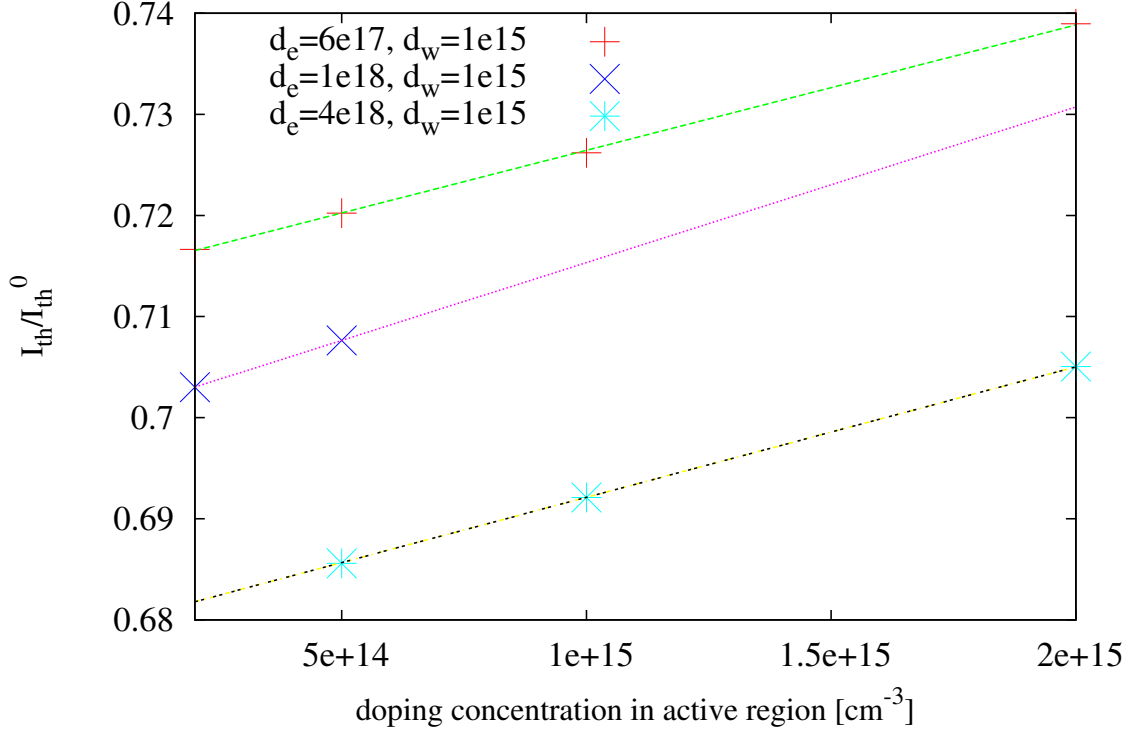


Figure 21: Threshold current (normalized by  $I_{th}^0$ ) as a function of carrier doping concentrations in active region, for a few values of concentration in emitters. Concentrations in waveguide regions is  $10^{15}/\text{cm}^3$ .

## 5.1 Active region doping

Figures 21 and 21 show the role of doping concentration in active region, for a few values of doping concentrations in emitter regions, on basic characteristics of lasers: threshold current and slope of light power versus current,  $dL(I)/dI$ , respectively.

We see that none of these quantities depends strongly on active region doping. These effects are similar to the one observed for "N-N" type of waveguide structure.

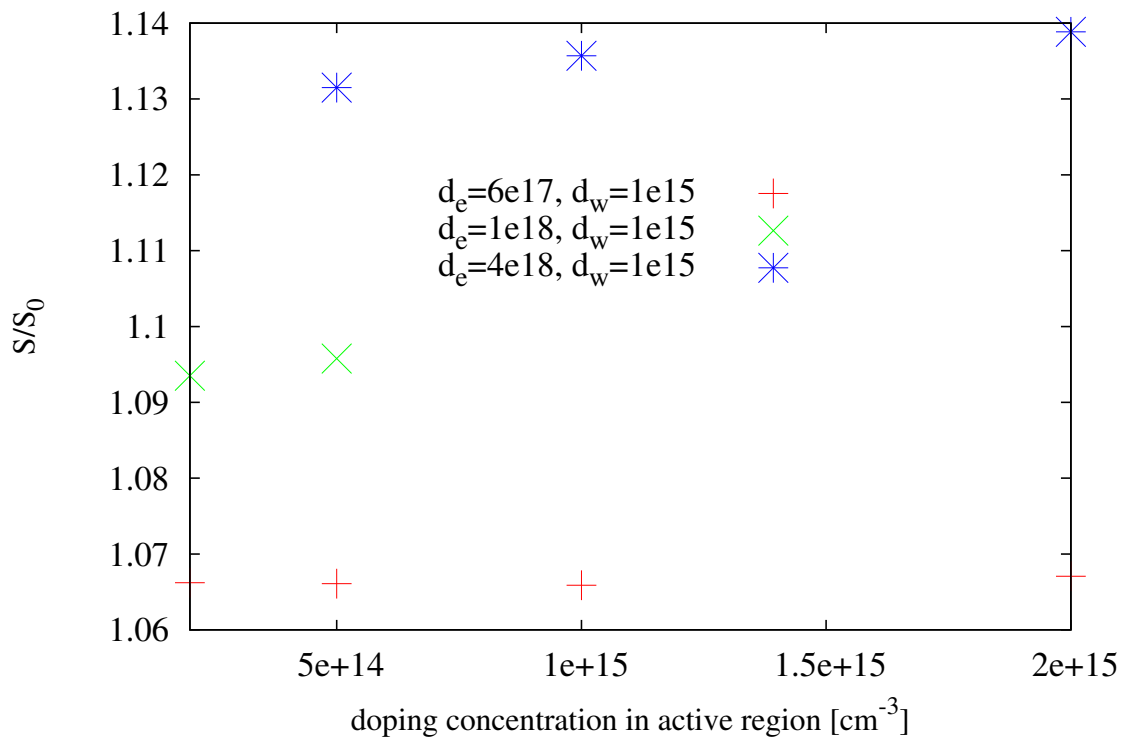


Figure 22: Slope of  $dL/dI$  (normalized by  $S_0$ ) for the data corresponding to these in Figure 21.

## 5.2 Waveguides doping

The effects of doping in waveguide regions are much stronger for N-P structure than these reported for N-N one.

Both, lasing threshold current (Figure 23) and corresponding  $dL/dI$  (Figure 23) show a nice strong linear dependence on waveguides doping. Since the first one has a positive slope and the second one negative, there will no maximum as a function of  $d_w$  in this case, which is different that for the case of N-N structure.

The lasing offset voltage  $U_0$  corresponding to the data displayed in Figures 23 and 24 does not change with waveguide doping (within the accuracy of our modeling, and the studied doping range), and it is of the value of  $1.711V$ .

In Figure 25 we compare optical efficiency for both types of structures.

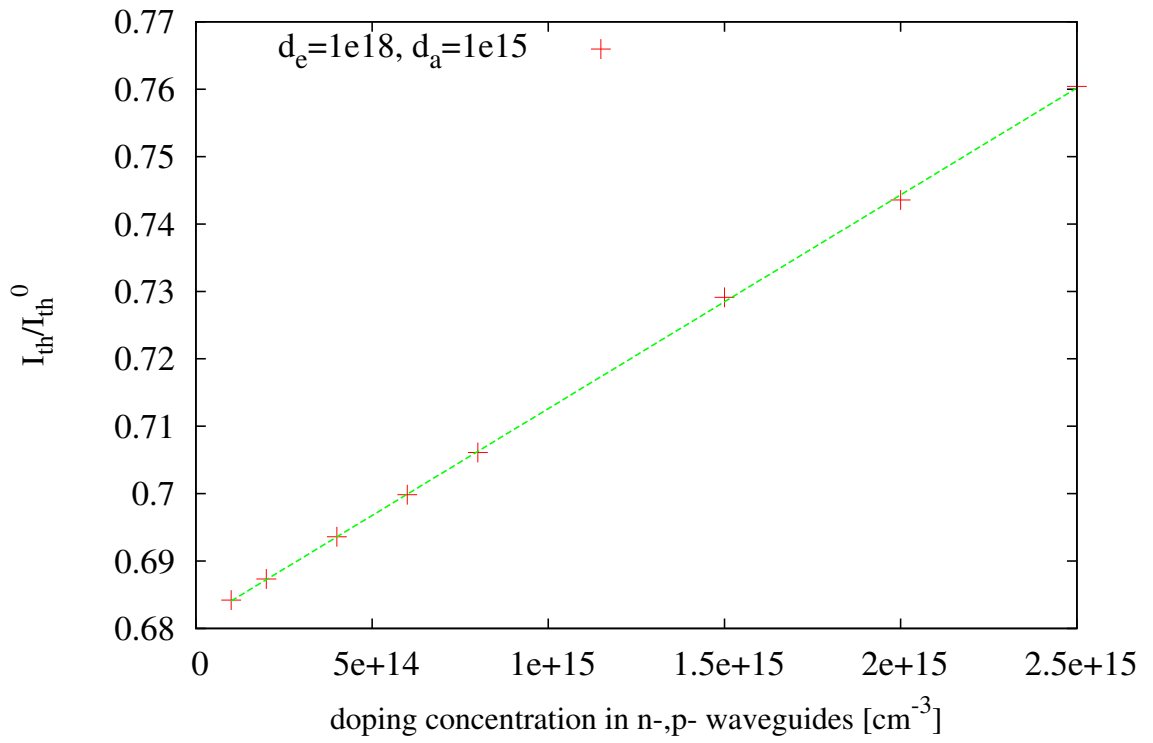


Figure 23: Threshold current (normalized by  $I_{th}^0$ ) as a function of carrier doping concentrations in waveguides. Concentrations in emitter regions are  $10^{18}/\text{cm}^3$  (n- and p-), and in active region it is  $n = 10^{15}/\text{cm}^3$ . The straight line is given by function  $f(x) = 3.17 \cdot 10^{-17} \cdot x + 0.681$ .

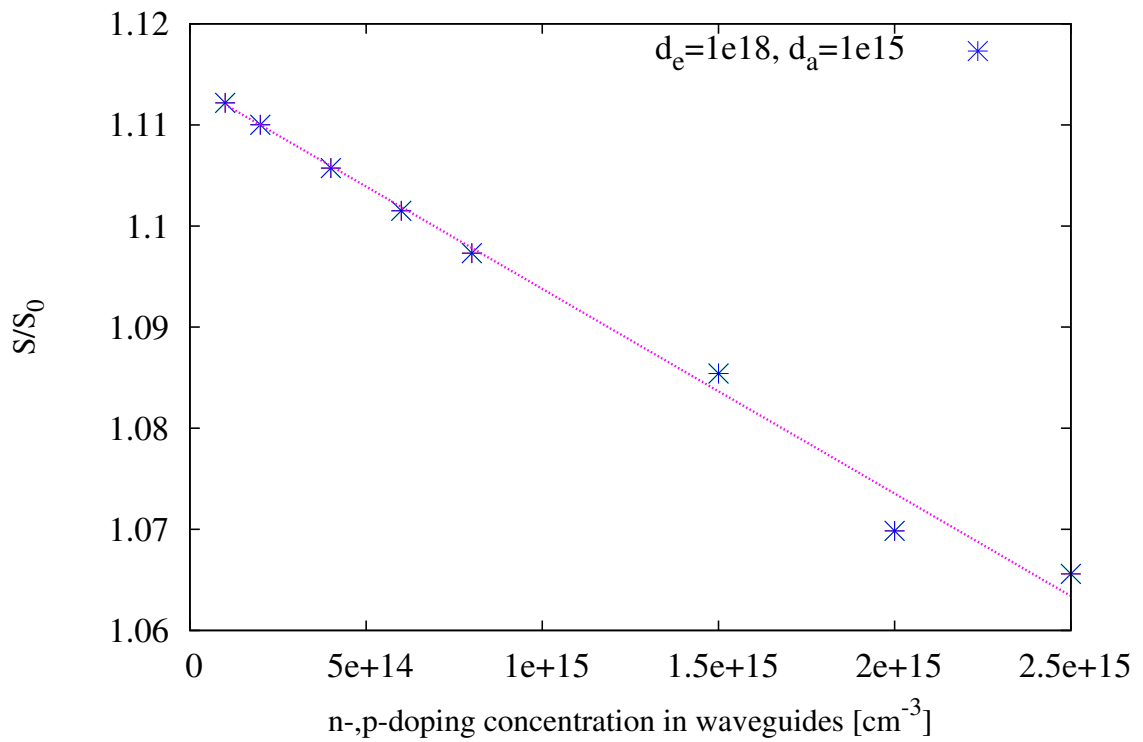


Figure 24: The slope of Optical Power,  $dL/dI$ , as a function of carrier doping concentrations in waveguides. Concentrations in emitter regions are  $10^{18}/cm^3$  (n- and p-), and in active region it is  $n = 10^{15}/cm^3$ . The straight line is given by function  $f(x) = -2.54 \cdot 10^{-17} \cdot x + 1.397$ .

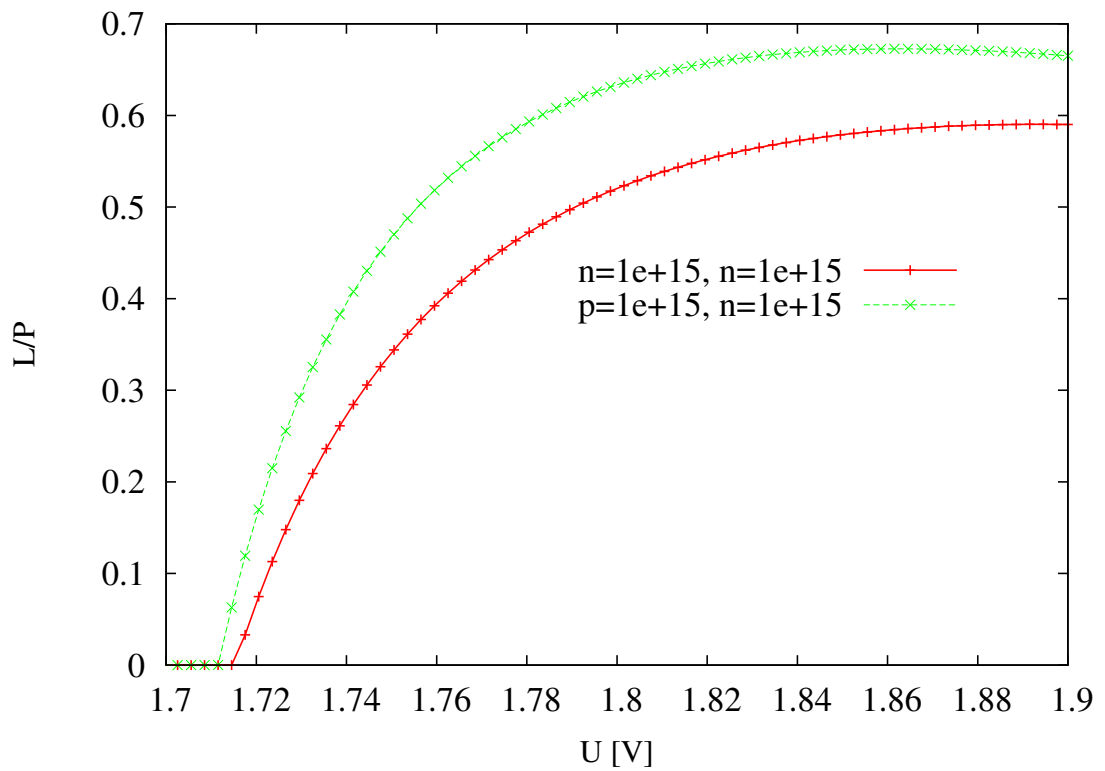


Figure 25: Optical efficiency as a function of voltage, for a few combinations of carrier doping concentrations in waveguides, as described in the Figure. Concentrations in emitter regions are  $10^{18}/cm^3$  (n- and p-), and in active region it is  $n = 10^{15}/cm^3$ .

### 5.3 Doping in Emitters

As in case on N-N structures, here also doping levels in emitters regions contribute the most to laser characteristics.

Figures 26 and 26 show example dependencies of  $I_{th}$  and  $dL/dI$  on doping in emitters. There are no maxima/minima there like in case of N-N structure, and at concentrations above about  $10^{18}cm^{-3}$  the effect of doping becomes small.

The lasing offset voltage  $U_0$  (Figure 28) is sensitive to emitters doping at low levels, only, below around  $10^{18}cm^{-3}$ . This is the same as for N-N structure.

Optical efficiency does depend weakly on doping at large doping levels, unlike for N-N structures (Figures 29 and 30).



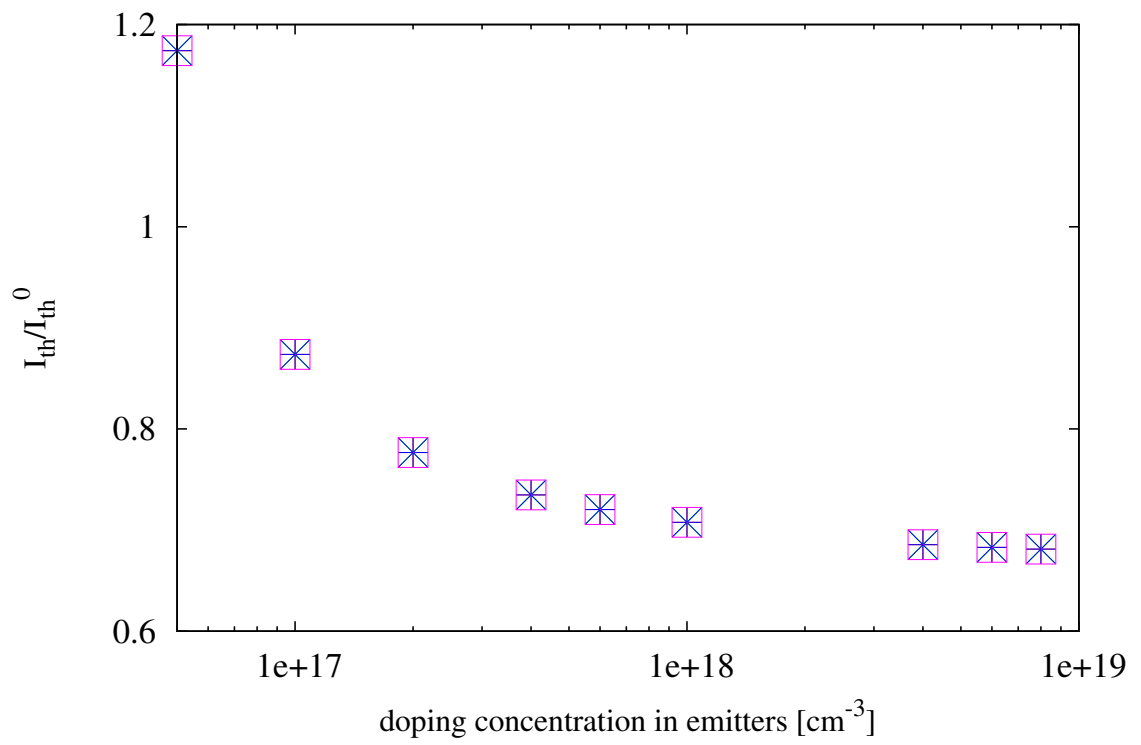


Figure 26: Threshold current as a function of carrier doping concentrations in emitters. Concentrations in waveguide and active regions are  $10^{15}/\text{cm}^3$

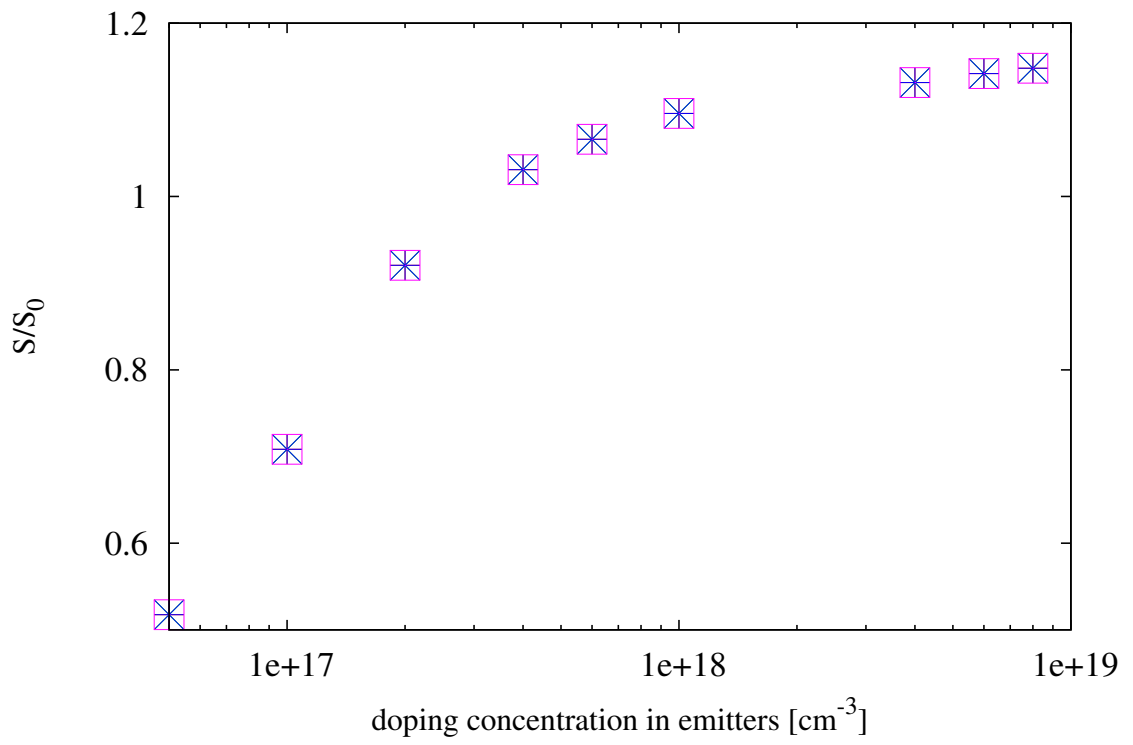


Figure 27: Slope  $dL/dI$  as a function of carrier doping concentrations in emitters. The data correspond to these in Figures 26 and 28.

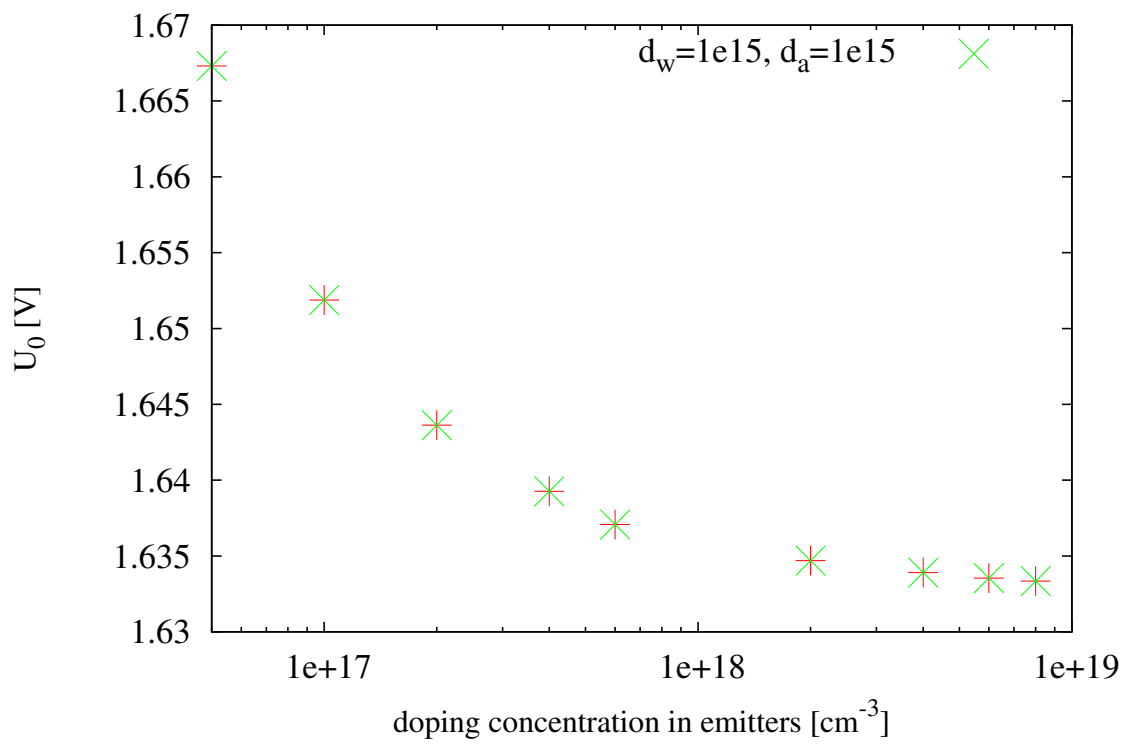


Figure 28: Lasing offset voltage as a function of carrier doping concentrations in emitters. The data correspond to these in Figures 26 and 27.

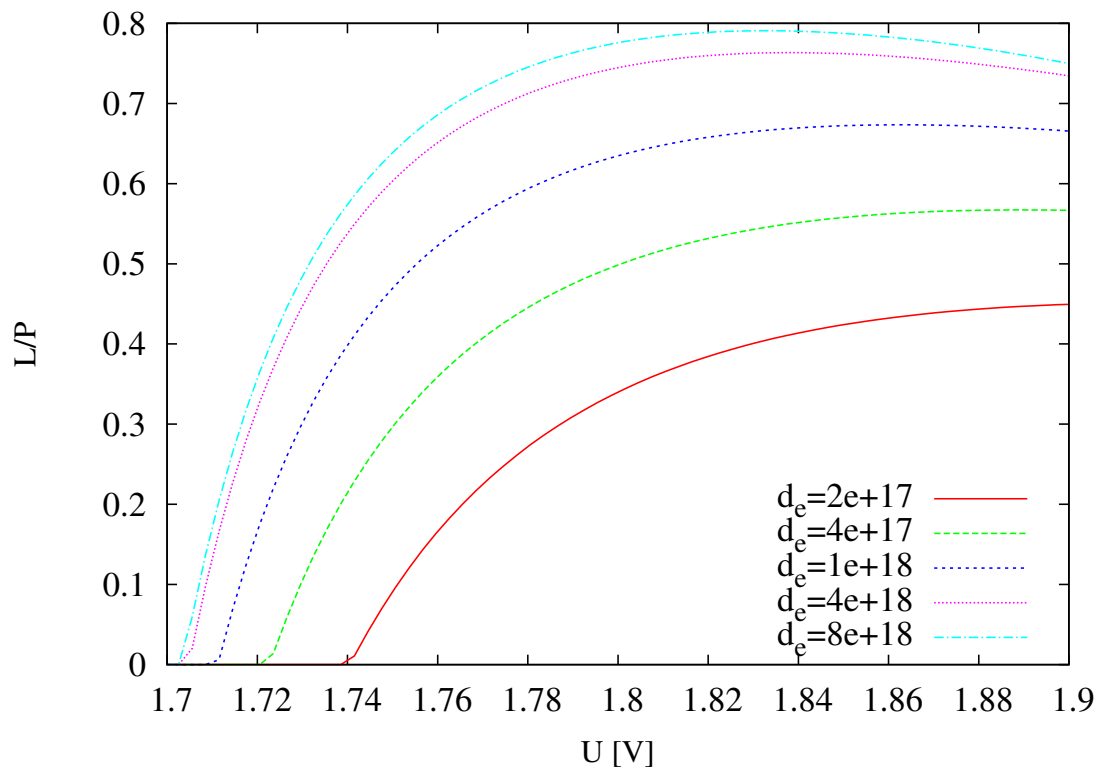


Figure 29: Optical efficiency for a few values of doping concentration in emitters. Concentration in waveguide regions is  $10^{15}/cm^3$  (n- and p-), and in active region it is  $n = 5 \cdot 10^{14}/cm^3$ .

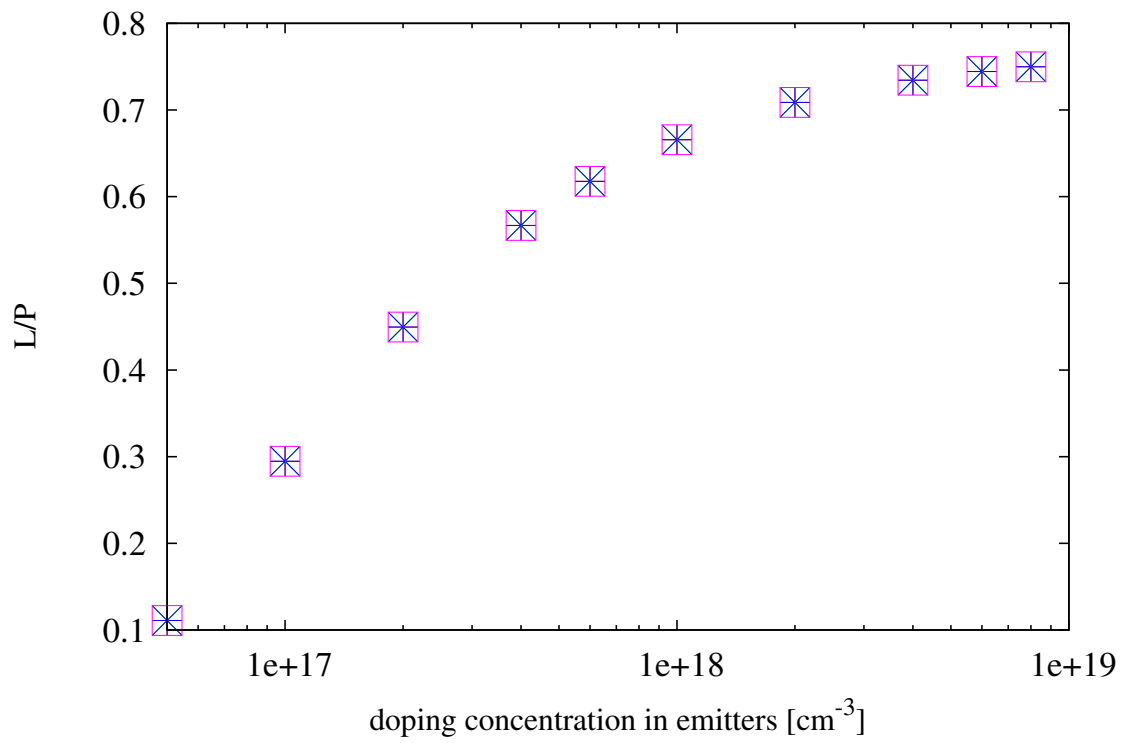


Figure 30: Optical efficiency at applied voltage of  $1.9V$ , as a function of doping concentration in emitters regions, when doping concentrations in waveguide is  $10^{15}/\text{cm}^3$  and in active regions it is  $5 \cdot 10^{14}/\text{cm}^3$ .

## 6 Summary and Conclusions.

SCH AlGaAs lasers with two kinds of waveguide doping structures have been modeled with Synopsys TCAD: "N-N" type structure where both waveguides have n-type of doping (with QW doping of n-type as well), and "N-P" structure where the waveguide on the side of p-emitter has p-type doping. The "N-N" structure is of the type we have experimental data for and it was used as a reference in our calculation calibration.

We observed that the doping level in active region has a small only influence on laser characteristics (lasing threshold current, slope of light power versus current, lasing offset voltage, optical efficiency). Better results are obtained for the lowest possible doping. More pronounced influence is of doping in waveguide regions. For "N-N" type of structure an optimal doping level is of around  $10^{15} \text{cm}^{-3}$ , but for "N-P" type of structure, it is desirable to have lower level of doping concentration there.

The most significant is the role of doping levels in emitters. It should be around  $10^{18} \text{cm}^{-3}$  in case of both types of structures. However, "N-P" type of structure gives significantly better results than "N-N" one, with threshold current lowered to about 70% and optical efficiency increased to near 80%.

## References

- [1] Zh. I. Alferov, *The double heterostructure concept and its applications in physics, electronics, and technology*, Rev. Mod. Phys. 2001. V.73. No.3. P.767-782.
- [2] S. I. Matyukhin, Z. Koziol, and S. N. Romashyn, *The radiative characteristics of quantum-well active region of AlGaAs lasers with separate-confinement heterostructure (SCH)*, arXiv:1010.0432v1 [cond-mat.mtrl-sci] (2010)
- [3] Z. Koziol, S. I. Matyukhin, *Waveguide profiling of AlGaAs lasers with separate confinement heterostructures (SCH) for optimal optical and electrical characteristics, by using Synopsys's TCAD modeling*, unpublished.
- [4] Z. Koziol, S. I. Matyukhin, and S. N. Romashyn, *Non-monotonic Characteristics of SCH Lasers due to Discrete Nature of Energy Levels in QW*, accepted for presentation at *Nano and Giga Challenges in Electronics, Photonics and Renewable Energy Symposium and Summer School*, Moscow - Zelenograd, Russia, September 12-16, 2011
- [5] A. Yu. Andreev, S. A. Zorina, A. Yu. Leshko, A. V. Lyutetskiy, A. A. Marmalyuk, A. V. Murashova, T. A. Nalet, A. A. Padalitsa, N. A. Pikhtin, D. R. Sabitov, V. A. Simakov, S. O. Slipchenko, K. Yu. Telegin, V. V. Shamakhov, I. S. Tarasov, *High power lasers ( $\lambda = 808$  nm) based on separate confinement AlGaAs/GaAs heterostructures*, Semiconductors, 2009, 43(4), 543-547.
- [6] A. V. Andreev, A. Y. Leshko, A. V. Lyutetskiy, A. A. Marmalyuk, T. A. Nalyot, A. A. Padalitsa, N. A. Pikhtin, D. R. Sabitov, V. A. Simakov, S. O. Slipchenko, M. A. Khomylev, I. S. Tarasov, *High power laser diodes ( $\lambda = 808 - 850$  nm) based on asymmetric separate confinement heterostructure*, Semiconductors, 2006 40(5), 628-632.
- [7] *Sentaurus Device User Guide*, Synopsys, 2010, [www.synopsys.com](http://www.synopsys.com)